X-ray Absorption and Resonant Inelastic X-ray Scattering Calculations with Ligand Field Single Cluster Method on Praseodymium Nickel Oxide

by

Shadi Balandeh

B.Sc., Sharif University of Technology, 2011

A THESIS SUBMITTED IN PARTIAL FULFILLMENT OF
THE REQUIREMENTS FOR THE DEGREE OF

MASTER OF SCIENCE

in

The Faculty of Graduate and Postdoctoral Studies

(Physics)

THE UNIVERSITY OF BRITISH COLUMBIA

(Vancouver)

October 2013

Abstract

RNiO3 perovskites (R=rare earth) are one of the most interesting compounds in condensed matter physics presenting various unusual physical properties. The detailed electronic structure of these materials are very controversial at the present time. The charge transfer energy and the d-d Coulomb interaction are the two very important parameters which can explain their electronic behaviours nicely. However, predicting their values has been a challenge to the science society so far.

X-ray Absorption Spectroscopy (XAS) and Resonant Inelastic Scattering (RIXS) are the two very useful techniques to probe the electronic structure of a solid state system in general and predict these two energies in particular. In this thesis Multiplet Ligand Field Cluster Calculation (MLFCC) is used to calculate these two spectra, then the charge transfer energy (Δ), the covalent hopping integral(pds), and the $d - d$ Coulomb repulsion energy Udd are obtained by fitting the calculated spectra to the experiment.

In this work, the calculated XAS results are compared with the experiment and the adjusted values are introduced as $\Delta = 2.5$ eV , pds=-1.9eV, Udd=7.5eV and 10Dq=0.5 eV.

The low spin to high spin transition is also studied and the critical charge transfer energies and covalent hopping integrals are calculated at which the abrupt transition happens. It is also found that in almost all low spin cases the d8L9 configuration has the largest contribution to the ground state. Since the best fit of XAS is not satisfactory and displays considerable differences with the experiment, the study is followed with the RIXS calculations.

Finally, the calculated RIXS results for different polarizations are compared with the experiment.It results in a smaller $\Delta = 0.8eV$ and a smaller absolute value of pds=-1.4eV at which the double peak structure in XAS L3 vanishes. This could be an evidence to the fact that XAS should not be interpreted in the conventional way and the Δ should not be fitted to keep the double peak which probably has another source than the multiplet structure.

Preface

The program has been used for the calculations is the "Ligand Field Theory Package"-version 2013.2.4 written by Maurits W.Haverkort.

The $PrNiO_3$ sample for the X-ray absorption spectra was grown at Max Planck Institute Stuttgart by G. Logvenov and G. Christiani and the corresponding measurement was carried out at the Canadian Light Source in Saskatoon by S. Macke, A. Radi, J. E. Hamann-Borrero, R. Sutarto and F. He and the first analysis including subtracting the background were done by S. Macke.

The Resonant Inelastic X-ray Spectroscopy (RIXS) experimental data are provided by Thorston Schmitt as the group leader and Valentina Bisogni both from Paul Scherrer Institute (PSI) and Marta Gibert, Sara Catalano and Jean-Marc Triscone all from the university of Geneva.

One of the high spin cobalt oxide X-ray absorption measurements in chapter 3 was carried out by Abdullah Radi in Canadian Light Source (CLS) with Ronny Sutarto and Sebastian Macke involved. The other CoO spectrum is provided by Dian Rata and Alex Frano from Berlin.

Table of Contents

List of Tables

List of Figures

Acknowledgments

First and foremost, I would like to express my sincere gratitude to my advisor Prof. George Sawatzky for the continuous support of my M.Sc study and research whilst allowing me the room to work in my own way, for his patience, contagious enthusiasm, and immense knowledge. I could not have imagined having a better advisor and mentor for my graduate study.

Besides my advisor, I would like to thank Prof. Maurits Haverkort for his patience and deep knowledge in answering my questions regarding his program and its physics.

I would also like to thank Dr. Sebastian Macke who was always willing to help and give his best suggestions. I also thank Abdullah Radi for training me on the X-ray diffraction machine and providing me with the TEY signal of CoO in the chapter three.

My sincere thanks also goes to Prof. Andrea Damascelli for his insightful comments on my thesis.

Last but not least, I would like to thank Dr. Ilya Elfimov for his support through the network technical issues.

Dedication

To my parents, Zohreh and Mohammad and to my brother, Mehrdad for their endless love and encouragement.

To the love of my life, my husband Ehsan for his continuous love and support.

Chapter 1

Background Materials

1.1 Transition Metal Oxides

Transition Metal Oxides (TMOs) are believed to be one of the most fascinating systems in solids. They exhibit various unusual physical properties such as the high temperature super conductivity, huge variations in their magnetic properties and metal-insulator transitions. The series $RNiO_3$ (R=Rare earth) are the transition metal oxides, which present a sharp insulator-metal transition strongly depending on temperature and tolerance factor.[19] Tolerance factor ($t \equiv \frac{d_{R-O}}{\sqrt{2}d_{Ni-O}}$) is used as a measure of the amount of distortion of a perovskite from an ideal cubic unit cell. Therefore, for a given $RNiO_3$, the closer the tolerance factor to one, the closer to cubic with Ni-O-Ni bond angle of $\theta = 180°$ .The detailed behaviour of these phase transitions are shown in Fig. 1.1
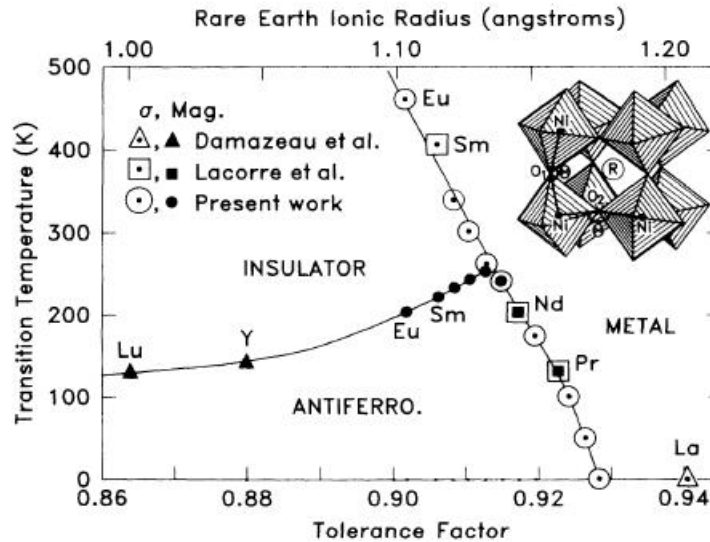
Figure 1.1: Insulator-Metal-Antiferromagnetic phase diagram for nickelates as a function of the tolerance factor or rare earth ionic radius and temperature.[19]

The phase diagram illustrates how for different rare earth radius, RNO shows different magnetic and electronic properties. These transitions distinguish three different regimes: Metal, anti-ferromagnetic insulator and paramagnetic insulator. From the diagram, it can be observed that at low temperatures, PrNiO3 shows anti-ferromagnetic behaviour with ordered anti-parallel spins, but when the temperature increases, it loses this ordering and experiences insulator-metal

transition with delocalized electrons.

The sensitivity of these physical properties to the crystal chemistry and structural distortions offers many possibilities to manipulating their properties in order to engineer new applications in these materials, such as in the complex oxides heterostructure. [23] But for this aim, the electronic structure of these materials itself has to be understood well.

From the Zaanen-Sawatzky-Allen scheme[21], using only a few parameters (the charge transfer energy and the $d - d$ Coulomb interaction energy) is able to account for the electronic behaviour of a great number of $3d$ TM oxides such as the phase transitions[13]. In this thesis we try to find these two parameters by fitting the Multiplet Ligand Field Single Cluster Calculations to the experiment. Another purpose of this work is to test this theoretical approach for the specific case of PrNiO3 (And NdNiO3) and comment if in this case the physical properties can be described reasonably well by a single cluster calculation or not and if not what the probable reasons could be.

In this thesis we also seek the charge transfer energy and the covalent hopping integral at which in a given d^7 valence configuration system a low spin to high spin transition can occur. Being in a low or high spin state is an important characteristic of a system which can control its magnetic and electronic properties.

The source of the unusual properties of d-transition metal oxides is the unique nature of the valence d electrons.
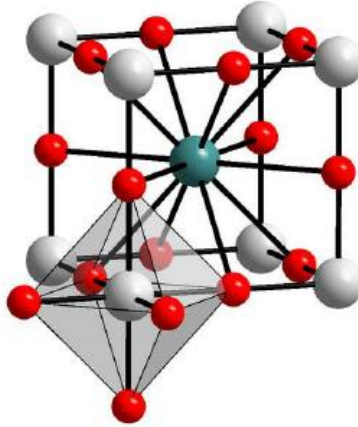
Figure 1.2: The atomic arrangement of a single unit cell of the perovskite crystal structure of RNO3. Green indicates the rare earth ion, red the oxygen and gray the nickel atoms.[3]

Transition metal atoms with their incomplete d shells combine with oxygen to form the transition metal oxides. These are relatively ionic compounds with O^{2-} ions and a rare earth in a 3+ valence state leaving the nickel also in a 3+ valence state. Therefore, in PNO, nickel is 3+ resulting in $3d^7$ valence shell configuration. Therefore, the principle quantum number n and the orbital angular quantum number l of the valence electrons are 3 and 2 respectively. In

a spherical potential, the electrons' wave functions can be expressed as:

$$\Psi_{n,l,m}(r,\theta,\varphi) = R_{n,l}(r)Y_l^m(\theta,\varphi) = R_{n,l}(r)p_l(\cos\theta)e^{im\varphi}$$

$R_{n,l}(r)$ are the radial part of the wave functions depending on the n and the l and $Y_l^m(\theta,\varphi)$ or the spherical harmonics are the angular part of the wave function depending on the magnetic quantum number m and the l which can be express in terms of the Legendre polynomials or $p_l(\cos\theta)$ with:

$$n = 1,2,3,...$$

$$l = 0,1,2,...,n-1$$

$$m = -l,-l+1,...,l-1,l$$

So for the d orbitals with $l = 2$, there are five different magnetic quantum numbers and therefore, five different angular wave functions, with:

$$-l \leq m \leq l \rightarrow -2 \leq m \leq 2 \rightarrow m = -2,-1,0,1,2$$

By using the corresponding spherical harmonics and the spherical to Cartesian coordinate conversion, the real parts of the angular d orbitals take the following forms:
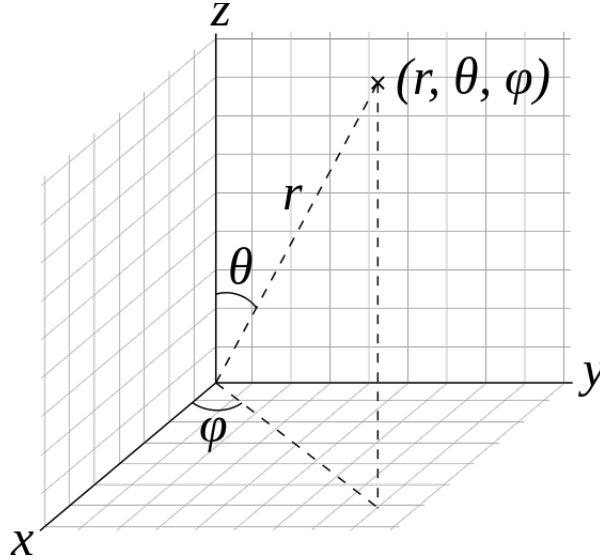
Figure 1.3: The spherical coordinates used in the spherical harmonics.[2]

$$x = r\sin\theta\cos\varphi$$

$$y = r\sin\theta\sin\varphi$$

$$z = r\cos\theta$$

$$Y_l^{m\star} = (-1)^m Y_l^{-m}$$

$$d(x^2 - y^2) \propto Re(Y_2^{-2}) \propto \sin^2\theta\sin 2\varphi = \frac{x^2 - y^2}{r^2}$$

$$d(yz) \propto Re(Y_2^{-1}) \propto \sin\theta\cos\theta\sin\varphi = \frac{yz}{r^2}$$

$$d(3z^2 - r^2) \propto Re(Y_2^0) \propto (3\cos^2\theta - 1) = \frac{3z^2 - r^2}{r^2}$$

$$d(zx) \propto Re(Y_2^1) \propto \sin\theta\cos\theta\cos\varphi = \frac{xz}{r^2}$$

$$d(xy) \propto Re(Y_2^2) \propto \sin^2\theta\cos 2\varphi = \frac{xy}{r^2}$$
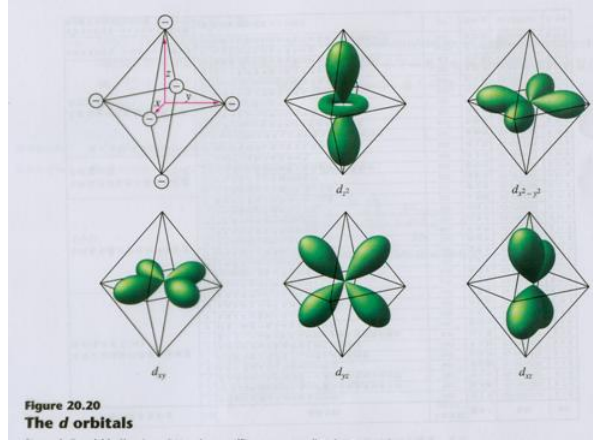
Figure 1.4: The real part of the angular wavefunctions of d orbitals.[5]

For zero magnetic field and neglect of the spin orbit coupling, energy does not depend on the magnetic quantum number m, therefore, in a spherical potential there are five different d wave functions with the same energy or in the other words, in a spherical potential, d orbitals are five-fold degenerate. Upon filling these states with electrons however one does have to take into account the Coulomb interaction between the electrons which develops into a complicated multiplet structure which we will discuss later in a simplified version.

However, to understand real materials, we are more interested in studying less symmetrical cases such as the octahedral potential in a single crystal of RNO, assuming a cubic crystal structure and equivalent Ni-O bond lengths. The lattice is shown in Fig. 1.2. One way to treat this group of potentials and geometries is using the Ligand Field Theory (LFT) where ligand usually refers to the oxygen 2p electron states forming bonds with the central Ni $3d$ states.

Crystal Field Theory (CFT) is the simplest form of LFT, in which each of the ligand ions is treated as a point charge. If consider each oxygen, as a negative point charge, then if the d orbitals points right towards them that will be very repulsive with a huge Coulomb repulsion energy and if they points between them, less repulsive. So when d orbitals are off-axis

$(d(xy), d(xz), d(yz))$ since oxygens are on the axes, it is less repulsive and in a lower energy.(Fig. 1.4). Therefore, The $d(x^2 - y^2)$ and $d(3z^2 - r^2)$ which are usually referred to as e_g orbitals, have the same and a higher energy and $d(xy)$, $d(yz)$ and $d(xz)$ or t_{2g} orbitals are found to be at a lower energy. That is how the degeneracy is partly removed in an octahedral geometry.

The splitting energy is usually referred as $10Dq$. The e_g orbitals go up by $6Dq$ and the t_{2g} orbitals go down by $4Dq$ to keep the center of gravity the same as for the spherical potential energy levels. The crystal field energy level diagram is shown in Fig. 1.5
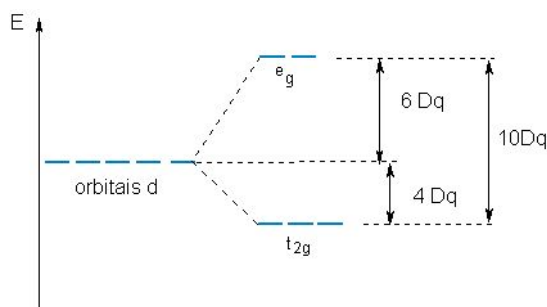
Figure 1.5: Crystal field energy level diagram for the octahedral geometry

1.2 Covalency

Although crystal field theory can explain some electronic features of the d orbitals, it completely ignores the nature of ligands by treating them as point charges.
That is why it fails in, for example, explaining a large energy splitting caused by a neutral ligand like CO or high spin to low spin transition by changing the charge transfer energy.

LFT is the model, which considers all ionic, covalent and hybridization aspects of coordination complexes.
The basic idea behind both CFT and LFT is that when there is a metal atom, mostly a transition metal ion, at the center of a coordination sphere, surrounded with donor ligand atoms, the energy of its valence orbitals is going to be changed by the existence of those ligands. Figures 1.5 and 1.6 show these two theories predictions in this regard in an octahedral geometry.

Apparently, there is a huge contribution from covalency and electron hopping between ligands and the metal ion. In the latter one, there are Ni-d orbitals at some energy and oxygen orbital at some lower energy. They interact with each other resulting in σ and π bonds and anti-bonds.

Fig. 1.7 shows how in cubic symmetry t_{2g} and e_g orbitals form π and σ combinations respectively. Since e_g orbitals point towards oxygens p orbitals, their hopping integrals are larger and put σ bonding and anti-bonding energies at higher levels than π ones. These hopping integrals are usually presented in the parameters $pd\sigma$ and $pd\pi$.
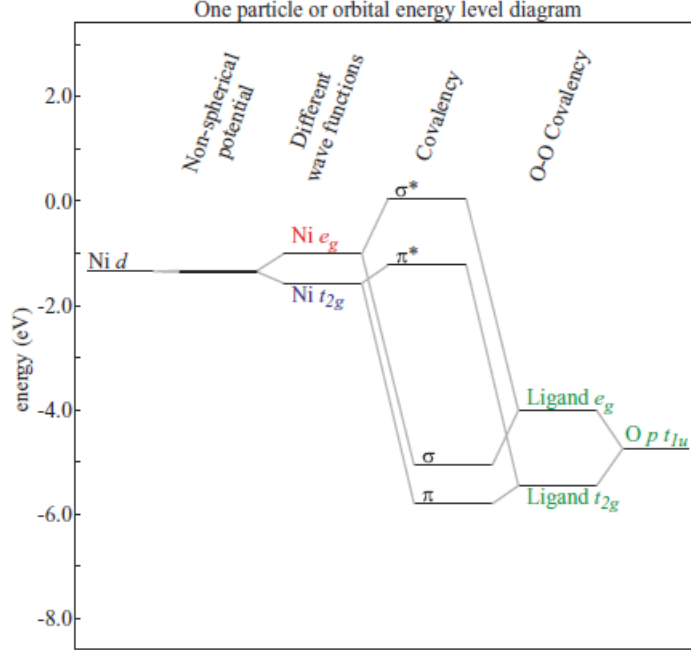
Figure 1.6: Orbitals energy level diagram for a NiO_6 cluster considering covalency and hybridizations.[8]
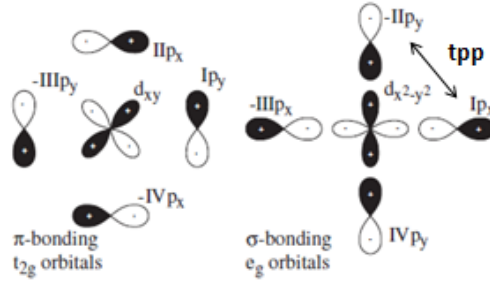
Figure 1.7: $d(xy)$ and $d(x^2 - y^2)$ orbitals forming π and σ bondings with oxygens' p orbitals respectively.[9]

tpp and *pds* are the other parameters related to the covalency which are defined as follows:[8]

$$tpp = pp\sigma - pp\pi$$

where $pp\sigma$ and $pp\pi$ are the σ type and π type hopping integrals between the oxygens p orbitals, defined relative to the O-O bond direction. In the other words, the bonding and anti-bonding orbitals are *tpp* below and above the O_p onsite energy.

V_{e_g} or *pds* and $V_{t_{2g}}$ are covalent hopping integrals are also defined as the follows:

$$V_{eg} = pds = \langle \psi_{d_{e_g}} | H | \psi_{L_{e_g}} \rangle = \sqrt{3} pd\sigma$$

$$V_{t_{2g}} = \langle \psi_{d_{t_{2g}}} | H | \psi_{L_{t_{2g}}} \rangle = 2pd\pi$$

Wherein $pd\sigma$ and $pd\pi$ are hopping energies between an electron in a Ni-d orbital and an electron in ligand-p shell with σ and π symmetries respectively. As an example consider the $d_{x^2-y^2}$ orbital with four π bonds with the oxygens p orbitals around in an xy plane as shown in Fig. 1.7 Then

$$V_{d_{x^2-y^2}} = \langle \psi_{d_{x^2-y^2}} | H | \psi_{L_{t_{2g}}} \rangle = \frac{1}{\sqrt{4}} [\langle \psi_{d_{x^2-y^2}} | H | p_1 \rangle + \langle \psi_{d_{x^2-y^2}} | H | p_2 \rangle + \langle \psi_{d_{x^2-y^2}} | H | p_3 \rangle + \langle \psi_{d_{x^2-y^2}} | H | p_4 \rangle]$$

$$= \frac{4}{\sqrt{4}} pd\pi = 2pd\pi$$

Where each p orbital has been considered normalized and $\frac{1}{\sqrt{4}}$ is the normalization factor for their linear combination. The signs in the linear combinations are determined by the orbitals phase and can be read off of the figure above. In defining the hopping integral the correct coordinate system has to be selected to preserve the symmetry.

1.3   The Zaanen-Sawatzky-Allen Model

There are two main theories describing the outer electrons. Theories which mostly can describe systems in which the band width is large compared to the electron-electron Coulomb repulsion energy. Alternatively, the systems in which there is a large overlap between the orbitals of neighbouring atoms such as the systems with s or p valence shell. The other ones are the theories which are more applicable to the systems with localized electrons and bandwidths smaller than the Coulomb energy like systems with outer f shells. [15]
Whereas the above systems, the TMOs with partially filled d shell, have an intermediate bandwidth and therefore show intermediate characters. That is why band theory or ligand field theory alone fails in describing them perfectly. One solution can be the employment of both theories together.

Before Fujimori[6] and Sawatzky and Allen[16] introduced charge transfer energy as an important parameter in the physics of transition metal oxides, it was thought for a long time that nickel oxide is a Mott-Hubbard insulator where the band gap is determined by U, the on-site $3d - 3d$ Coulomb repulsion energy. But it was not consistent with the experiments which presented huge differences in the band gap for the compounds with a same TM atom and different surrounding ions.[10] If it was a Mott-Hubbard insulator, the band gap should be determined by the U_{dd}, which is not changed strongly with changing the ions. This controversy was settled by considering Δ, the energy it costs to transfer an electron from a ligand to the transition metal atom. Zaanen, Sawatzky and Allen presented a systematic scheme [21] interpreting the electronic structure of the $3d$ transition metal compounds in terms of the Δ

and the U_{dd}.

According to ZSA diagram, Fig. 1.8, there are two different types of gaps possible in transition metal compounds. Namely, the charge transfer gap due to the ligand to metal charge transfer energy and the Mott-Hubbard gap associated with Coulomb interaction energy. Then associated with these two gaps, the compounds can be categorized into two regimes: Mott-Hubbard regime where U is smaller than Δ and the band gap is determined by the U, and charge transfer regime where Δ is smaller than U and the magnitude of band gap is given by Δ. Therefore, it can be concluded that when either the Mott-Hubbard gap or charge transfer gap closes, there will be an insulator to metal transition. The diagram of their density of states is shown in Fig. 1.9 which illustrates their differences in more details. Fig. 1.10 also shows what kind of charge fluctuations happen in each of these two types of materials.
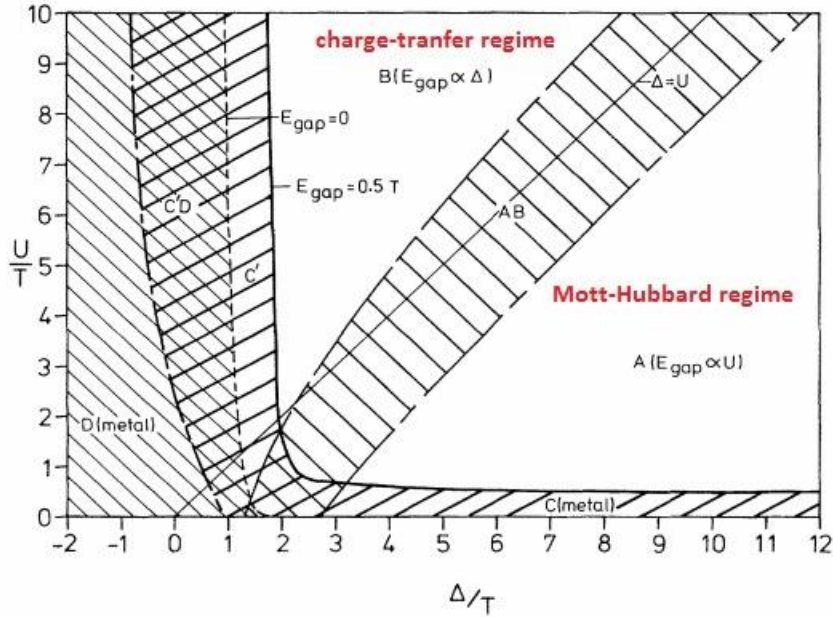
Figure 1.8: The Zaanen-Sawatzky-Allen (ZSA) diagram[21]

The on-site effective screened $3d-3d$ Coulomb energy U or U^{eff} is here defined as the energy it costs to transfer an electron from a TM d orbital to another TM d orbital on a different site. So, basically we are left with a d^{n+1} and a d^{n-1} ions rather than the two initial d^n ions. In order to find the U or the Hubbard conductivity gap, the Hund's ground state energies 1.4 of the systems with n, $n-1$ (ionized state), and $n+1$ electrons (electron-affinity state) have to be calculated.[12]

$$U = E(d^{n+1}) + E(d^{n-1}) - 2E(d^n)$$

The charge transfer energy (Δ) is an energy it costs to remove an electron from a ligand p

(a) Mott-Hubbard insulator
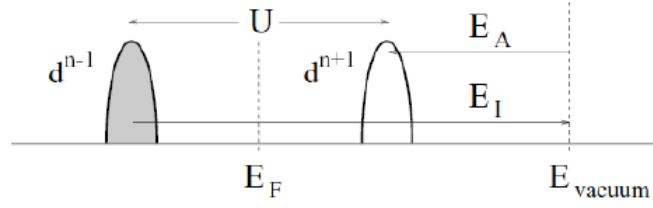
(b) Charge transfer insulator
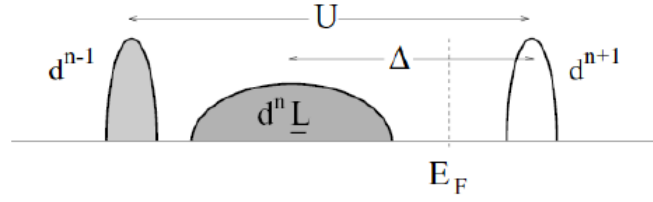
Figure 1.9:   Density of states versus energy of TM $3d$ and anion $2p$ states determining the two different types of insulator in ZSA scheme. E_A and E_I are electron affinity and ionization energies.[17]
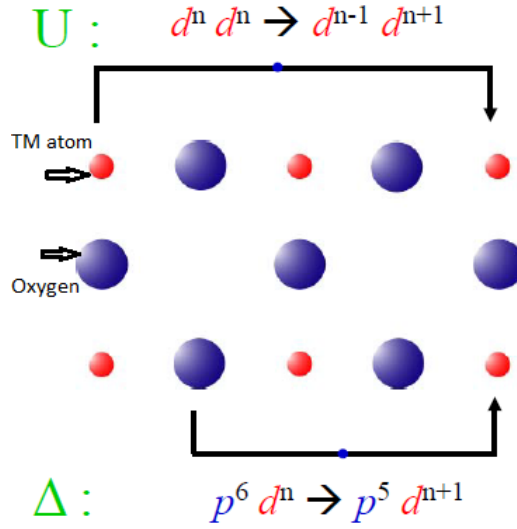
Figure 1.10: Electron removal and addition in Mott-Hubbard insulator and charge transfer insulators.[17]

orbital and put it in a TM d orbital.

$$\Delta = E(d^{n+1}\underline{L}) - E(d^n)$$

where $\underline{L}$ denotes one hole in a ligand atom.

It is believed that high valence oxides like Ni^{3+} in RNOs belong to the charge transfer regime where the smallest gap is associated with the ligand to metal charge transfer energy. Therefore, it should be strongly affected by the configurations of the transition metal and its surrounding oxygen ions.

That could be the reason makes $RNiO_3$ electronic structure difficult to understand and challenging. In this thesis we try to investigate this for Praseodymium Nickel Oxide (PNO) by doing Ligand Field Cluster Calculations (LFCC), employing M. W. Haverkorts codes[9] and experimental data from CLS and PSI.

1.4 Multiplets and Hund's Rules

The Hund's rules determine in a given system which state should be the ground state. They say that the atomic orbitals of a particular shell have to be filled according to the following rules:

Firstly, the total spin has to be maximized. It in fact implies that the electrons should have parallel spins. Therefore, from the Pauli exclusion principle they must be in different spatial orbitals which results in a smaller Coulomb repulsion and lowers the energy.

Secondly, the total orbital angular momentum has to be maximized. It leads to having lots of angular lobes which again reduces the Coulomb repulsion.

And the third one states that for the less than half filled shells the total angular momentum is $J = L - S$ and for more than half filled shells, it is $J = L + S$

Then the Hund's ground state energy can be determined by:[12]

$$E(n, Hund) = \alpha_I(n)I + \alpha_{F_0}(n)F^0 + \alpha_J(n)J + \alpha_C(n)C$$

where: $\alpha_I = n$, $\alpha_{F^0} = \frac{n!}{2}$ and the α_J is the number of parallel spin pairs and I is the one electron potential. C describes the angular part of the multiplet splitting and J is the Hund's exchange interaction energy which describes the exchange interactions between parallel spins:

$$C(dd) = \frac{1}{14}(\frac{9}{7}F^2 - \frac{5}{7}F^4)$$

$$J_H(dd) = \frac{1}{14}(F^2 + F^4)$$

In Multiplet Ligand Field Theory (MLFT), there are several possible electronic configurations (multiplets) with different energies because of the different Coulomb interaction energies for each. These electron-electron Coulomb interactions can be written as:[18]

$$\langle\psi|\sum_{i,j>i}^{N}\frac{1}{r_{ij}}|\psi\rangle = \binom{N}{2}\langle\psi|\frac{1}{r_{12}}|\psi\rangle$$

In Hartree-Fock formalism the many body wavefunctions $|\psi\rangle$ are chosen to be in the form of the Slater determinant, so with P's as permutation operators, we will have:

$$|\psi\rangle = \frac{1}{\sqrt{N!}} \begin{vmatrix} \psi_1(\vec{x_1}) & ... & \psi_N(\vec{x_1}) \\ \psi_1(\vec{x_2}) & ... & \psi_N(\vec{x_2}) \\ ... & ... & ... \\ ... & ... & ... \\ \psi_1(\vec{x_N}) & ... & \psi_N(\vec{x_N}) \end{vmatrix} = \frac{1}{\sqrt{N!}} \sum_{n=1}^{N!} P_n\{\psi_1(\vec{x_1})...\psi_N(\vec{x_N})\}$$

$$\langle\psi|\frac{1}{r_{12}}|\psi\rangle = \frac{1}{N!} \sum_{n,m=1}^{N!} \int (-1)^{n-1} P_n\{\psi_1^\star(\vec{x_1})...\psi_N^\star(\vec{x_N})\}\frac{1}{r_{12}}(-1)^{m-1}P_m\{\psi_1(\vec{x_1})...\psi_N(\vec{x_N})\}d\vec{x_1}d\vec{x_N}$$

$$= \frac{(N-2)!}{N!} \sum_{n,m=1}^{N} [\int \psi_n^\star(\vec{x_1})\psi_m^\star(\vec{x_2})\frac{1}{r_{12}}\psi_n(\vec{x_1})\psi_m(\vec{x_2})d\vec{x_1}d\vec{x_2} - \int \psi_n^\star(\vec{x_1})\psi_m^\star(\vec{x_2})\frac{1}{r_{12}}\psi_n(\vec{x_2})\psi_m(\vec{x_1})d\vec{x_1}d\vec{x_2}]$$

$$\Rightarrow \langle\psi|\sum_{i,j>i}^{N}\frac{1}{r_{ij}}|\psi\rangle = \frac{1}{2}[\sum_{m\neq n}^{N} \int \psi_n^\star(\vec{x_1})\psi_n(\vec{x_1})\frac{1}{r_{12}}\psi_m^\star(\vec{x_2})\psi_m(\vec{x_2})d\vec{x_1}d\vec{x_2}$$

$$- \int \psi_n^\star(\vec{x_1})\psi_m(\vec{x_1})\frac{1}{r_{12}}\psi_m^\star(\vec{x_2})\psi_n(\vec{x_2})d\vec{x_1}d\vec{x_2}] = \langle nn|mm\rangle - \langle nm|mn\rangle$$

Note that in the first integral the $\psi_n^\star(\vec{x_1})\psi_n(\vec{x_1})$ and $\psi_m^\star(\vec{x_2})\psi_m(\vec{x_2})$ terms are like the classical charge densities of two electrons in orbital n and m so the whole integral acts like the classical Coulomb repulsion. But the second term has no classical counterpart and comes from the "Pauli exclusion principle". It is subtracted from the first term and reduces the total Coulomb repulsion energy compared to the classical case. They are usually referred as *Slater integrals* and *exchange term* respectively.

These two terms can also be expressed in one term as:

$$V_{ijkl} = \int \int \frac{1}{|r_1 - r_2|} \psi_i^\star(r_1)\psi_j^\star(r_2)\psi_k(r_2)\psi_l(r_1)dr_1dr_2$$

It is convenient to express this integral in terms of the Legendre polynomials and the spherical harmonics:

$$R^k(ij,kl) = \int \int \frac{2r_<^k}{r_>^{k+1}} P_i^\star(r_1)P_j^\star(r_2)P_k(r_1)P_l(r_2)dr_1dr_2$$

where $r_< = min(r_1,r_2)$, $r_> = max(r_1,r_2)$

However, the Coulomb interaction term is usually expressed in *Slater integrals* as: $F^k(i,j) = R^k(ij,ij)$ and $G^k(i,j) = R^k(ij,ji)$ which are corresponding to the Coulomb term and exchange term respectively. It can be derived that for electron-electron interaction in d orbitals all terms

except F^0, F^2 and F^4 vanish, these are usually called monopole, dipole and quadrupole integrals respectively. Because of the polarizations effect the monopole term (F^0) is strongly screened and reduced. For example, in NiO it is about 7 eV[20], while its atomic value is about 18 eV.[14] . In our calculations it is referred as U_{dd} which is varied to get the best agreement with experiment. The other Slater terms are hardly reduced because of the screening so we can trust the *abinitio* results for them. Although experience shows that better is reduce them by about 20% because of the atomic correlation effects and the hybridization with ligand orbitals in the compounds.

In transition metal chemistry these Slater integrals are usually expressed in terms of Racah parameters A, B and C with:

$A = F_0 - 49F_4$

$B = F_2 - 5F_4$

$C = 35F_4$

With $F_0 \equiv F^0, F_2 \equiv \frac{F^2}{49}$ and $F_4 \equiv \frac{F^4}{441}$

In MLFT the energy of a state with n electrons in an open d shell is determined by:

$$E(n, L, S, \lambda) = nI + \frac{1}{2}n(n-1)U_{av} + U(n, L, S, \lambda)$$

Wherein, L, S and λ are total orbit, spin and seniority quantum numbers. I is the one electron potential, U_{av} is the average multiplet Coulomb exchange interaction energy and $U(n, L, S, \lambda)$ is the multiplet splitting.

The average Coulomb repulsion energy between two electrons in a d orbital in terms of Slater integrals is:

$$U_{av} = F^0 - \frac{14}{441}(F^2 + F^4)$$

1.5 2p-X-ray Absorption Spectroscopy

In 2p-XAS, a hole is created in a $2p$ core level by transition of an electron from there to $3d$ valence shell by shining x-ray photons to the sample. This excited state is very unstable so the core hole decays by radiant x-ray emission or other radiation-less transitions like Auger decay.[7]

There are many different states in the valence shell but only transitions obeying dipole selection rules can happen. Therefore for each initial state the set of available excited states are different. That is why 2p-XAS can provide good information of the electronic structure of the ground state.

The rate of transition from the initial state i to the final state f through the above process

can be determined by the Fermi's Golden rule:

$$R_{i \to f} = \sum_f \frac{2\pi}{\hbar} |\langle f|A.p|i\rangle|^2 \delta(E_f - E_i)$$

Where p is the momentum operator and A is the vector potential of the applied electromagnetic field. The delta term satisfies energy conservation and the sum is over all unoccupied final states with the energies of E_f. Then it can be seen that to have a finite transition probability we need to have specific conditions in the initial and final states. As an example, the transition from a s orbital to p_y orbital with x polarized light is not allowed since the corresponding matrix term is zero which is an integral over an odd function over whole space. This also explains why XAS spectra can be different for different light polarizations (but not in the cubic symmetry).

In this report, 2p-XAS is used to study a nickelate single cluster in PNO.

To understand XAS main features, let us take a look at Fig. 1.11 which is a PNO XAS spectrum from experiment. There are two resonance structures near energies 853 and 870 eV.
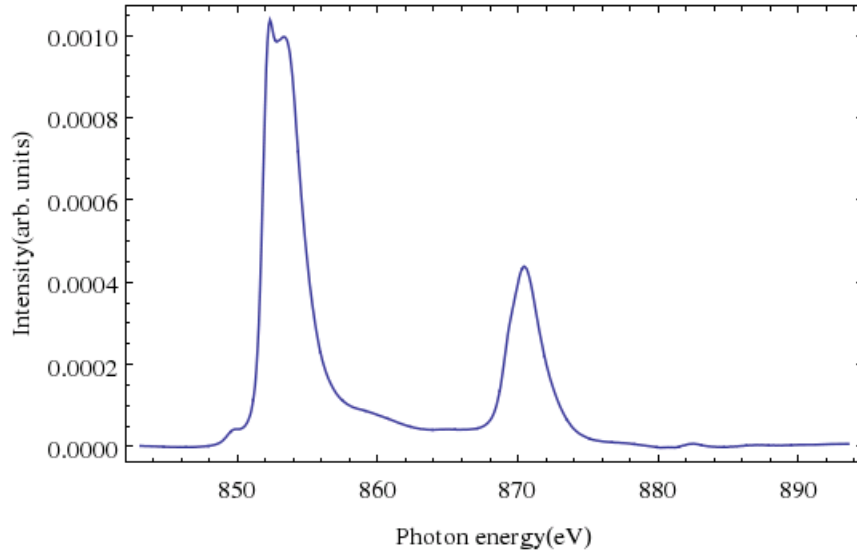
Figure 1.11: PNO 2p-XAS spectra from experiment [11]

Therefore, there is a 17 eV energy difference between them. This cannot be due to the splitting energy between t_{2g} and e_g orbitals. This splitting is only about 1eV or less. The splitting between these two peaks, which are called L_3 and L_2, with L_3 at a lower energy,is resulted from the spin orbit coupling in the 2p-core level.

The spin-orbit coupling is an interaction between electron's spin magnetic moment and the magnetic field generated by the electron's orbital motion around the nucleus. These interaction energy is equal to:

$$\Delta H = \mu_s.B_l$$

13

The electric field electrons travel through is radial so from the Biot-Savart law the magnetic field will be:

$$B = \frac{Ze\mu_\circ}{4\pi r^3}[v \times r]$$

$$l = r \times m_e v$$

$$\rightarrow B = \frac{Z_{eff}e\mu_\circ}{4\pi r^3 m_e}\vec{l}$$

$$\mu_s = -g_s\frac{e}{2m_e}\vec{s}$$

$$\rightarrow \Delta H = \frac{Z_{eff}e^2\mu_\circ}{8\pi m_e^2}\frac{1}{r^3}(\vec{s}.\vec{l})$$

We also have:

$$\langle\frac{1}{r^3}\rangle \propto Z_{eff}^3$$

$$\rightarrow \Delta H = \lambda\vec{s}.\vec{l}$$

with $\lambda \propto Z_{eff}^4$ where Z_{eff} is the screened nuclear charge.

The orbital angular momentum in $2p$ shell is 1 and spin of a single hole is $\frac{1}{2}$ so the associated total angular quantum number can take the following range of values:

$$|l - s| \le j \le |l + s| \rightarrow \frac{1}{2} \le j \le \frac{3}{2} \rightarrow j = \frac{1}{2}, \frac{3}{2}$$

These two values give rise to the two different resonance peaks.

$$J = L + S \rightarrow J^2 = L^2 + S^2 + 2L.S \rightarrow j(j+1) = l(l+1) + s(s+1) + 2l.s$$

$$\langle\lambda l.s\rangle = \lambda\frac{j(j+1) - l(l+1) - s(s+1)}{2}$$

$$= \frac{\lambda}{2}[j(j+1) - 1(1+1) - \frac{1}{2}(\frac{1}{2}+1)] = \lambda 2[j(j+1) - \frac{11}{4}] =$$

$$for j = \frac{1}{2} \rightarrow = -\lambda$$

$$for j = \frac{3}{2} \rightarrow = \frac{\lambda}{2}$$

$$\Rightarrow splitting : \frac{3\lambda}{2}$$

We saw earlier that the coefficient λ is proportional to Z_{eff}^4. Therefore this splitting in the 2p-XAS spectra should increase strongly with increasing the effective nuclear charge.

The Fig. 1.12 shows how for late transition metal compounds with higher nuclear charge the $L_3 - L_2$ splitting is larger compared to the early transition metal ones. There is a same
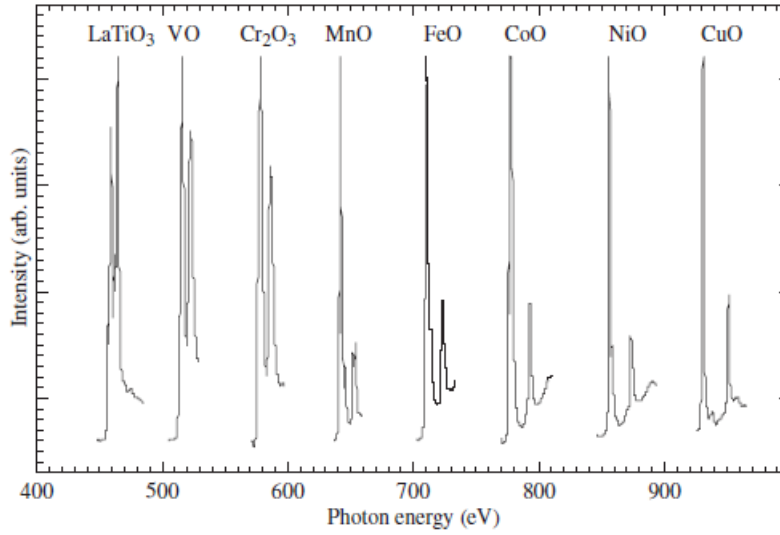
Figure 1.12: 2p-XAS spectroscopy of different transition metal compounds. The $L_3 - L_2$ splitting is larger for the late transition metal compounds with the higher nuclear charges. [9]

trend for transition metals with $3d$, $4d$, $5d$ and $6d$ configurations. The higher Z_{eff} the larger spin-orbit coupling effect.

L_3 corresponding to $j = \frac{3}{2}$, has higher intensity because of the higher degeneracy of $2j+1 = 4$ comparing $2j + 1 = 2$ in L_2. In 1.11 the continuum steps in background intensity, which are from excitations to unbound continuum-like state, have been subtracted. In XAS, the spectral shape can also provide detailed information of the ligands' effect on the metal and the atom's electron configuration. As discussed above the energy splitting is also an indication to the spin-orbit coupling effect.

Another feature of a spectrum is its spectral line width. The spectral lines are not infinitely sharp. They are broadened and one of the most important reason of this broadening is called the "'life-time" or the "'natural"' broadening. The reason is rooted in the "'uncertainty principle' which relates the excited state life time to the uncertainty of its energy. The shorter life time, the larger energy uncertainty or the wider spectral line. The experimental energy resolution is the another source to the line width broadening.

1.6 Resonant Inelastic X-ray Scattering

RIXS is a powerful tool to probe low energy excitations such as the charge transfer and $d - d$ excitations.

In this process the photon makes an excitation from core to conduction band, then an electron decays back from conduction band to the core and a photon comes out. The excitations in which an electron decays back to the same d configuration are called $d - d$ excitations and those falling to another configuration with different number of d electrons and ligand holes are

known as charge transfer excitations. [7]

Therefore, This process should not be necessarily elastic. The second electron can decay from a lower level in the conduction band and photon can lose some energy. The amount of lost energy depends on the occurred excitation. Fig. 1.13 shows how different kind of excitations cost different amount of energies,the energy scales are relevant for transition metal oxides. The process is resonant because energy of the incident light has to be the same as the energy of the x-ray absorption edges to excite an electron from core to valence.

RIXS usually is considered as a two-step process. One from initial state $|i\rangle$ to an intermediate one $|m\rangle$ and then from intermediate to final state $|f\rangle$ with the energies of E_i, E_m and E_f respectively. The intermediate state is the state with a hole in the core level, which is the same as the excited state in XAS.

The corresponding intensity of this second order process is determined by the Kramers-Heisenberg (KH) formula:

$$I \propto \sum_f \left(\sum_m \frac{\langle f|T^\dagger|m\rangle\langle m|T|i\rangle}{E_i + \hbar\Omega - E_m - \frac{i\Gamma_m}{2}} \right)^2 \delta(E_i - E_f + \hbar\Omega - \hbar\omega)$$

Ω and ω are angular frequencies of the incident and emitted photons respectively. Γ_m is the intermediate state intrinsic line-width or the broadening due to the intermediate state lifetime and T is the relevant transition operator. At resonant, when the intermediate state is the XAS final state, the other terms in the denominator become zero $(E_m - E_i = \hbar\Omega)$ and leaves only the core-hole broadening.
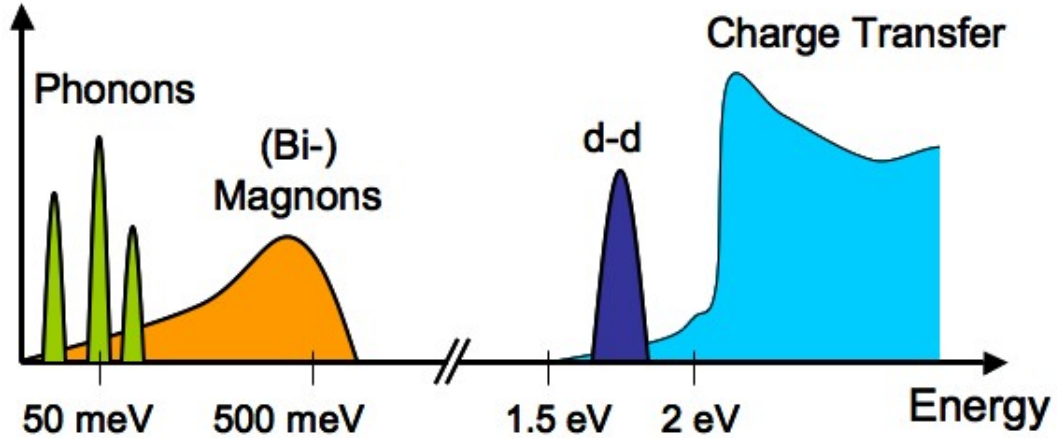
Figure 1.13: Low energy excitations in a condensed matter system. The energy scales are relevant for transition metal oxides.[1]

Chapter 2

XAS calculations

2.1 Configuration Interaction Model in a Single Cluster Calculation

In a configuration interaction model, the wave functions for the single cluster are expressed as a linear combination of different possible configurations.[22] In PNO, where a nickelate single cluster is going to be studied, nickel has d^7 valence shell electron configuration and p^6 core shell. NiO cluster has six oxygens around so there are $3 * 6 = 18$ $O - p$ orbitals. But, not all linear combinations are taken into account, only those that couple and interact with Ni-d orbitals are considered. Based on the Goodenough-Kanamori hybridization rules the number of them is reduced to ten, because for each Ni-d orbital there is one such linear combination. In this case either one, two or three electrons can hop from ligand to nickel d orbitals.

So the XAS ground state wavefunction can be expressed as:

$$\psi_g = \alpha_1 |p^6 d^7 L^{10}\rangle + \alpha_2 |p^6 d^8 L^9\rangle + \alpha_3 |p^6 d^9 L^8\rangle + \alpha_4 |p^6 d^{10} L^7\rangle$$

$p^n d^m L^z$ denotes n electrons in the transition metal core p shell, m electrons in the transition metal ion d shell and z electrons in the ligands' p shell.

The dimension of Hamiltonian matrix that has to be diagonalized can be obtained as follows:

$p^6 d^7 L^{10}$: p shell is full so there is only one possible configuration here, there are seven electrons in the ten d orbitals so there are $\binom{10}{7} = 120$ ways to arrange them there. Ligand orbitals are also full with ten electrons so there is only one possible configuration there. Therefore, there will be $1 * 120 * 1 = 120$ possible states for this configuration.

With the same counting, there will be 450, 450 and 120 states corresponding to $p^6 d^8 L^9, p^6 d^9 L^8$ and $p^6 d^{10} L^7$ configurations respectively. Therefore, there are 1140 wavefunctions altogether and a 1140×1140 Hamiltonian matrix.

And for the XAS state since one electron is excited from Ni-p shell to the Ni-d shell the excited wavefunction will be presented as:

$$\psi_{XAS} = \beta_1 |p^5 d^8 L^{10}\rangle + \beta_2 |p^5 d^9 L^9\rangle + \beta_3 |p^5 d^{10} L^8\rangle$$

Again with the same counting there will be 270, 600, 270 states corresponding to $p^5 d^8 L^{10}, p^5 d^9 L^9$ and $p^5 d^{10} L^8$ configurations so there are again $270 + 600 + 270 = 1140$ wavefunctions in total.

Due to the multiplet effect which is rooted in electron-electron interactions, these 1140

final states do not all have the same energies. They spread out over an energy range. Each configuration has its own multiplet and set of final states, which differ from one element to another.

Using ligand orbitals reduces the Hilbert space significantly and increases MLFT calculations efficiency.[8]

There are some important parameters that will be introduced in the following paragraphs. Many of them can be calculated *abinitio* like dipole and quadruple Slater integrals, and some will be adjusted to experiment, which we mostly deal with in this thesis.

U_{dd} and U_{pd}: The monopole Coulomb interactions which are strongly reduced because of the screening in a polarizable medium. They will be fitted to experiment to obtain the best agreement. U_{dd} is the one between electrons in Ni-d shell and U_{pd} is between the Ni p-core hole and Ni-d electrons. From what has been discussed in the previous chapter, U_{3d-3d} is given by:

$$U_{3d-3d} = E(d^6 L^m) + E(d^8 L^m) - 2E(d^7 L^m)$$

Where $E(d^n L^m)$ is the center of gravity of the $d^n L^m$ multiplets.

For multiple interactions or Slater integrals F^2 and F^4 ,the screening is not huge. Because they do not involve in changing the charge of ions. Therefore, they can be obtained *abinitio* from calculations and reduced by about 20%.

The line width broadening, G: It is the energy broadening parameter as introduced in the previous chapter.1.5

Charge transfer energy Δ: Another very important parameter in these calculations specifically, and in transition metal oxides generally, is the charge transfer energy or Δ. As it was introduced in the last chapter,1.3 it is the energy cost to hop one electron from the ligand to the metal d shell. In this case, it is the difference between on-site energy of $d^7 L^{10}$ and $d^8 L^9$ configurations. With this definition, the on-site energies for each configurations can be expressed in terms of Δ and the monopole Coulomb repulsion energies, U_{dd} and U_{pd} and the bare on-site energies of electrons in each shell, ϵ_p, ϵ_d and ϵ_L as follows:
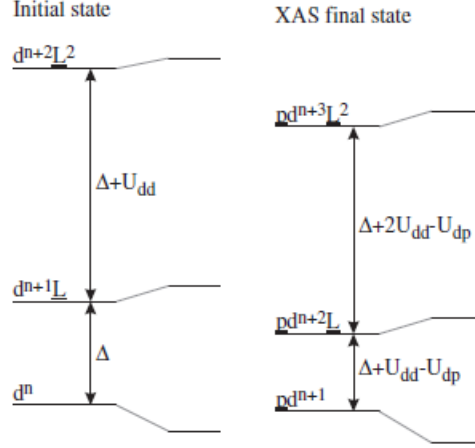
Figure 2.1: The relative on-site energies of the different configurations for the initial and final states in 2p-XAS in terms of Δ, U_{dd} and U_{pd} [9]

Ground state conf.	On-site energy	Relative on-site energy
$p^6 d^7 L^{10}$	$6\epsilon_p + 7\epsilon_d + 10\epsilon_L + \binom{7}{2}U_{dd}$	0
$p^6 d^8 L^9$	$6\epsilon_p + 8\epsilon_d + 9\epsilon_L + \binom{8}{2}U_{dd}$	$\epsilon_d - \epsilon_L + 7U_{dd} \equiv \Delta$
$p^6 d^9 L^8$	$6\epsilon_p + 9\epsilon_d + 8\epsilon_L + \binom{9}{2}U_{dd}$	$2\Delta + U_{dd}$
$p^6 d^{10} L^7$	$6\epsilon_p + 10\epsilon_d + 7\epsilon_L + \binom{10}{2}U_{dd}$	$3\Delta + 3U_{dd}$

Table 2.1: Ground state configurations and the corresponding energies.

Excited state conf.	On-site energy	Relative on-site energy
$p^5 d^8 L^{10}$	$5\epsilon_p + 8\epsilon_d + 10\epsilon_L + \binom{8}{2}U_{dd} - \binom{8}{1}U_{pd}$	0
$p^5 d^9 L^9$	$5\epsilon_p + 9\epsilon_d + 9\epsilon_L + \binom{9}{2}U_{dd} - \binom{9}{1}U_{pd}$	$\Delta + U_{dd} - U_{pd}$
$p^5 d^{10} L^8$	$5\epsilon_p + 10\epsilon_d + 8\epsilon_L + \binom{10}{2}U_{dd} - \binom{10}{1}U_{pd}$	$2\Delta + 3U_{dd} - 2U_{pd}$

Table 2.2: Excited state configurations and the corresponding energies

After basis sets are defined, operators as matrices and wavefunctions as vectors also have to be created in order to start the calculations. In this case they are created in cubic (O_h) symmetry.

2.2 Seeking the Best Agreement with Experiment

Now we can set numerical values to the introduced parameters and generate the XAS spectra. We seek the best agreement with the experiment. To this aim, for each parameter, in a reasonable range of values the calculations are repeated in small steps. The best fitting is happened at the following values: $pds = -1.9$, $tpp = 0.8$, $U_{dd} = 7.5$, $U_{pd} = 9.0$, $10Dq = 0.5$, $\Delta = 2.5$, $G = 1eV$. The final match corresponding to the above values are shown in Fig. 2.2 The criteria for goodness of fit are mostly the intensity ratio between between the peaks in L_3 (in the double peak structure), the line shape and the spin orbit coupling splitting energy.

For each set of values, besides the XAS spectrum, the expectation values of some other quantities are also calculated, which are presented at the top of each spectrum. N_{eg}, $N_{t_{2g}}$ and N_d are the average numbers of electrons in d_{e_g} and $d_{t_{2g}}$ orbitals and their sum in the d shell respectively. The square of the coefficients α_1, α_2, α_3 and α_4 are also calculated. As they have been defined earlier, they are the indications of each configuration contribution to the ground state.

$$\psi_g = \alpha_1|p^6d^7L^{10}\rangle + \alpha_2|p^6d^8L^9\rangle + \alpha_3|p^6d^9L^8\rangle + \alpha_4|p^6d^{10}L^7\rangle = \alpha_1|\psi_7\rangle + \alpha_2|\psi_8\rangle + \alpha_3|\psi_9\rangle + \alpha_4|\psi_{10}\rangle$$

$$P_7 = |\langle\psi_7|\psi_g\rangle|^2 = \alpha_1^2$$

$$P_8 = |\langle\psi_8|\psi_g\rangle|^2 = \alpha_2^2$$

$$P_9 = |\langle\psi_9|\psi_g\rangle|^2 = \alpha_3^2$$

$$P_{10} = |\langle\psi_{10}|\psi_g\rangle|^2 = \alpha_4^2$$

$$\sum_{i=1}^{4} P_i = \alpha_1^2 + \alpha_2^2 + \alpha_3^2 + \alpha_4^2 = 1$$

By comparing the calculated and experimental spectra, it can be seen that other than some very general features like the spin-orbit coupling splitting, the other details do not agree. The splitting in calculated L_3 peak is smaller than the experiment. The line shapes in both peaks do not match very well and the shoulder in the calculated L_3 peak is not present in the experiment. The differences are shown more clearly in Fig. 2.3 of the L_3 peaks alone. The differences are even more considerable in Fig. 2.4 which the calculation is done with the smaller broadening of 0.2 eV (compared the previous 1 eV broadening) which is in fact more realistic. There are at least three significant multiplet structure peaks which are not present in the experiment.

While it is usually believed that the d^7L^{10} configuration has the largest contribution to the ground state[13] , it is found in our calculations that in the final result, d^8L^9 configuration has a larger contribution number than d^7L^{10} with α_2^2 larger than 50% .It is an important result as

it can be the reason why the calculations do not work well here.

That perhaps is an indication that the cluster is not big enough, because it seems that the starting point should have been the starting point in which we start with nickel d^8 configuration and a hole in the oxygens and then we can no longer use a single local cluster because all the other nickels are also contributing ligand holes. for example in $Pr^{3+}NiO_3$ the nickel would be 2+ rather than the former 3+, and there will be one hole per each three oxygens or two holes for the whole single octahedron with six oxygens and that is not included in our Hilbert space. These holes can propagate and form bands with other clusters which are not included in the Hilbert space of a single cluster calculation either.

It might sound strange that how with a positive Δ, the ground state wavefunction has a larger d^8L^9 contribution than the d^7L^{10}, which basically indicates the d^8L^9 state has a lower energy than the other one. The explanation is hidden in the definition of the Δ. As it has been defined earlier, it is an *average* energy difference between the two states and does not include crystal field splitting. It is simply defined in terms of the single particle energies which are kind of an average energy, ϵ_d and ϵ_L, and monopole Coulomb interaction energy, U_{dd} and does not include the other Coulomb terms either. But the truth is, each of these states has many multiplets and therefore there are many energy differences between these two states. Apparently there must have been a particular d^8L^9 multiplet with a lower energy than a d^7L^10 multiplet.

$tpp = 0.8,\ pds = -1.9,\ 10Dq = 0.5,\ U_{dd} = 7.5,\ U_{pd} = 9,\ \Delta = 2.5,\ Distortion = 0,\ Broadening = 1.\ eV$

$N_{e_g} = 1.707,\ N_{t_{2g}} = 5.966,\ N_d = 7.673$

$\alpha_1^2 = 0.411,\ \alpha_2^2 = 0.508,\ \alpha_3^2 = 0.079,\ \alpha_4^2 = 0.002$
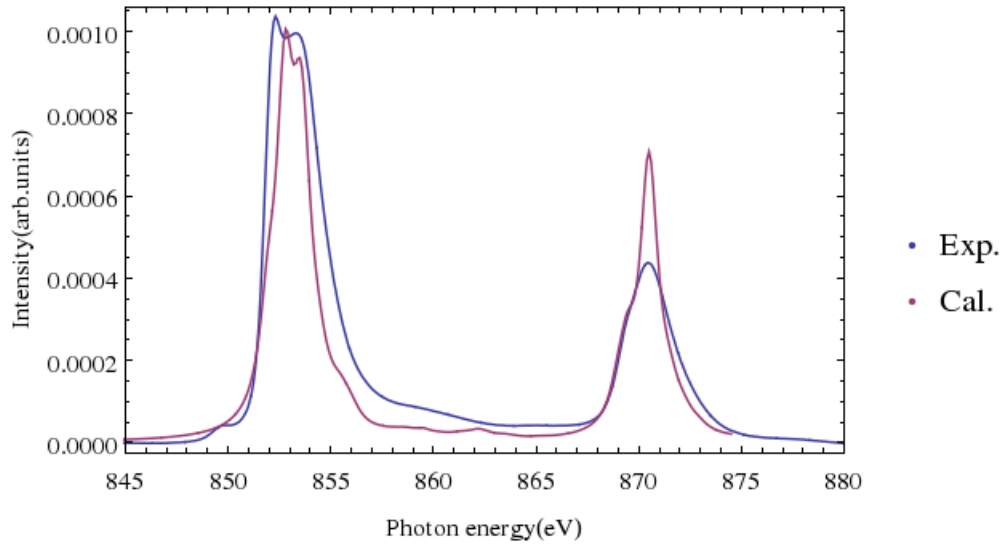
$S^2 = 1.031$

Figure 2.2:   The final calculated XAS spectra comparing the experiment
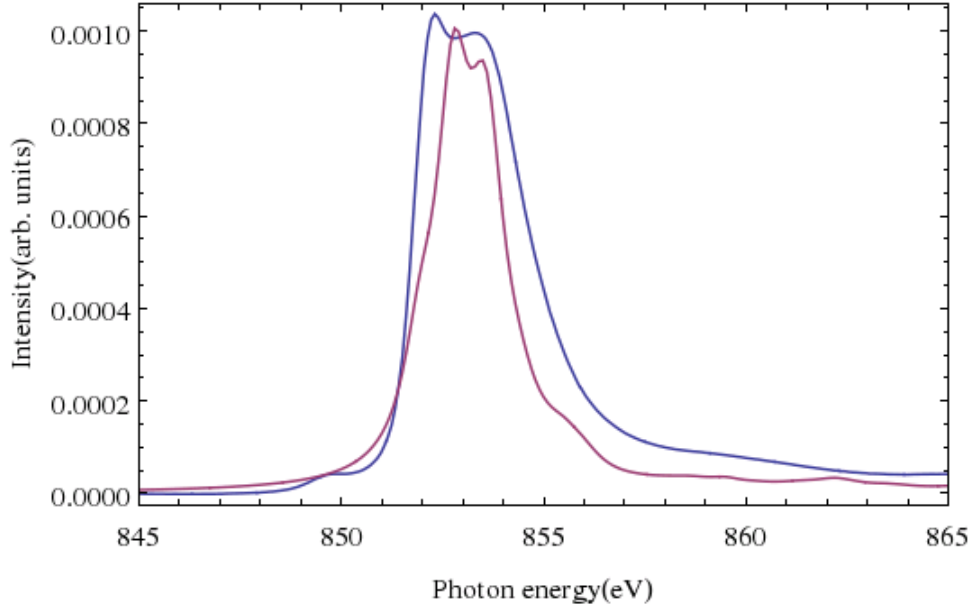
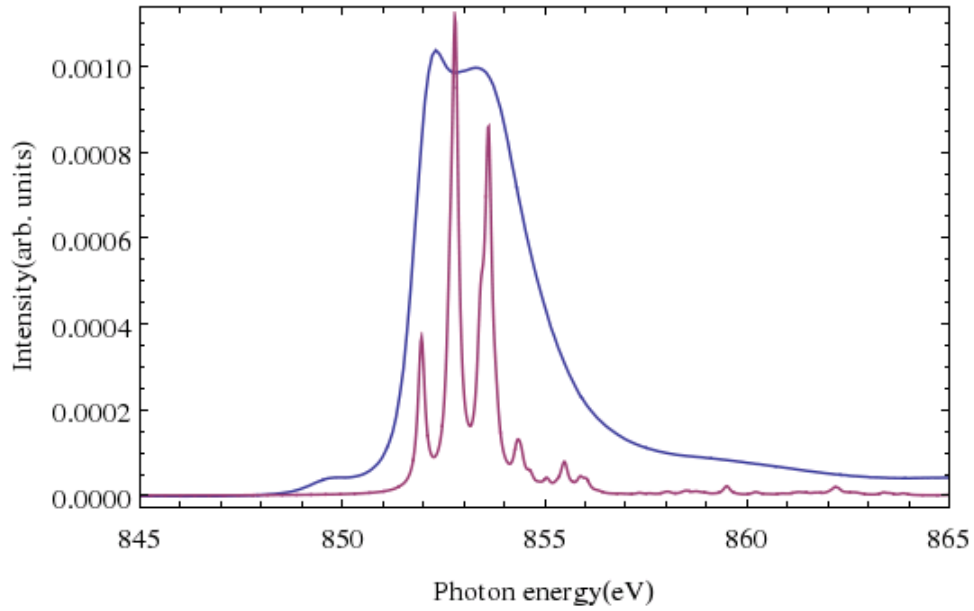Figure 2.3: Comparing the L_3 peaks in the calculations and the experiment

Figure 2.4: The same calculated L_3 peak with the lower broadening of 0.2 eV compared with experiment

Chapter 3

Spin State Transition

3.1 Introduction

It is generally accepted that if Ni is in a d^7 state in these materials it is most likely in a low spin state contrary to what it for example is in NiO where it is in a high spin state. The spin state is of course of great importance in describing the magnetic properties but also the electronic structure. So we should check if the XAS spectrum matches a high spin or a low spin state. To study this I present a brief introduction to the spin state transition that would occur if we change the parameters for example to a very large charge transfer energy . I also then compare the XAS spectra to demonstrate that we must be in a low spin state which provides limits to the charge transfer energy and the covalent hopping integral pds.

Fig. 3.1 is a simpler illustration of Fig. 1.6 which shows the energy levels of the d-transition metal oxide in an octahedral geometry considering the covalency.
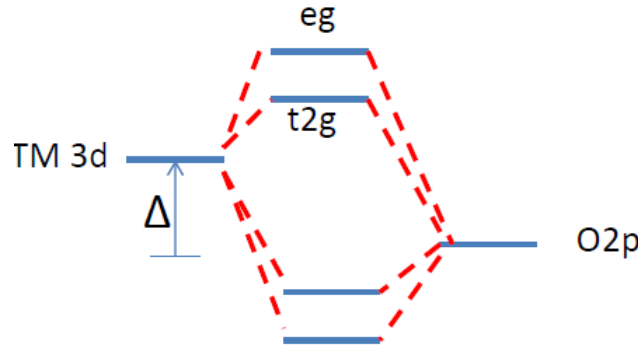
Figure 3.1: The energy levels of a d-transition metal oxide in an octahedral geometry considering the covalency with surrounding oxygens.

in perturbation theory for large delta compared V_{eg} the splitting is determined by:

$$splitting\ energy = \frac{V_{eg}^2 - V_{t_{2g}}^2}{\Delta}$$

The parameters are defined in the first chapter.

Now Fig. 3.2 shows how by decreasing the Δ or increasing the pds or V_{eg}, which increases the splitting energy, the system can experience an abrupt transition from a high spin state to a low spin state ,as dictated by Hund's rule.
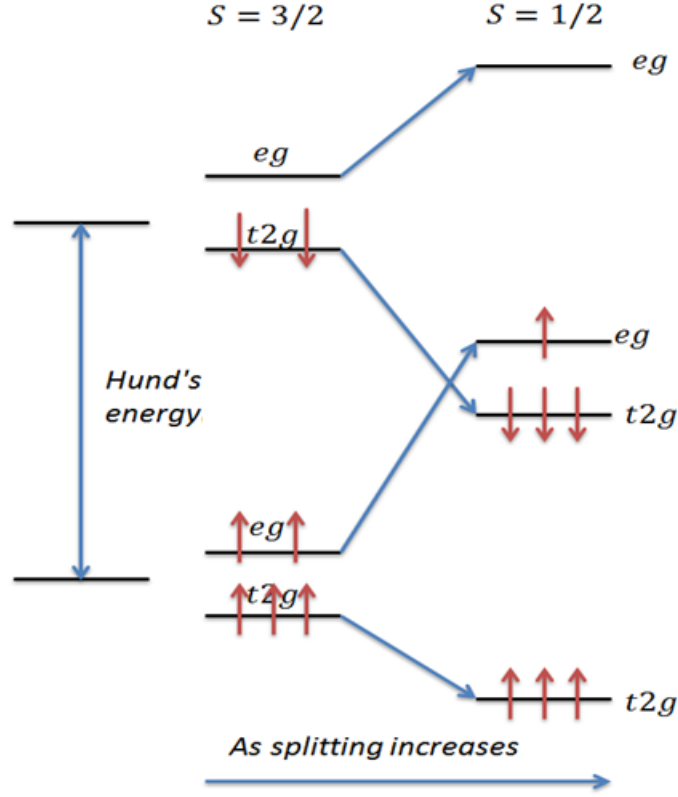
Figure 3.2: It shows how by decreasing the charge transfer energy, splitting increases and subsequently system changes from High spin State to Low spin State.

Apparently, this transition can occur when the low spin state has a lower energy than the high spin one. These energies can be determined by the Hund's energy expression as follows: In both cases the number of electrons or n is the same so only the Hund's exchange energy and on-site energies are going to be considered:

$$E(HS) = -\binom{5}{2}J + 5(-4Dq) + 2(6Dq) = -10J - 8Dq$$

$$E(LS) = -2\binom{3}{2}J + 6(-4Dq) + 6Dq = -6J - 18Dq$$

To HS to LS transition:

$$-6J - 18Dq < -10J - 8Dq$$

$$4J < 10Dq$$

Therefore, when the energy $4J$ is smaller than the energy $10Dq$ the low spin state has a lower energy and the spin transition can occur.

3.2 Low Spin to High Spin Transition

In this section the critical values of the hopping integrals and the charge transfer energy wherein PNO experiences a transition from low spin to high spin states, are obtained and discussed.

The expectation value of S^2 operator in the ground state is also calculated, which should basically be $s(s + \frac{1}{2})$. As it has been discussed in the previous section the total spin squared value in a nickelate single cluster is either 3.75 in the high spin state or 0.75 in the low spin state while the calculated numbers here are either about 3 in HS or about 1 in LS. The reason is hidden in the program's spin operator definition and calculation. Here the total spin operator only acts on the nickel atom not on the whole cluster including the ligands and that is why the numbers differ. But they can still be an indication for the spin state .

In changing the parameters most changes in the shape of the spectra are continues and gradual except at some points in changing the Δ and pds. At some certain values even a 0.05 eV change in them alters the shape drastically. It is also true that at those points the spin value abruptly changes from about 1 to about 3. So it seems that at those specific values of Δ or pds, the material changes from low spin to high spin state and that is why it also shows a very different behaviour in its XAS. Fig.3.3 and 3.4 are the spectra just before and after the transition with increasing Δ only by 0.05 eV from 3.75 to 3.80 eV and Fig. 3.5 and 3.6 are the ones with changing the pds by 0.05 eV from -1.65 to -1.60 eV.

Remember, at this point, the fitting does not matter any more, here we only care about the spin state for any d^7 system with the $d-d$ Coulomb energy of 7.5 eV, 10Dq of 0.5 eV and a zero distortion which also gives us limits to the charge transfer energy and the covalent hopping integral pds in our low spin system.

It is worth looking at another high spin d^7 system to compare the high spin XAS spectra with. In Fig. 3.7 you may find the XAS spectra for high spin cobaltate which is a d^7 high spin material. [4] It can be observed that the both high spin systems show some similar behaviours in their XAS line shapes.

As it explained above by increasing Δ or decreasing the absolute value of pds the splitting energy decreases and system experiences a low spin to high spin transition (3.2) So for each specific value of Δ there is a specific critical value of pds which can produce the needed splitting energy to make the spin transition and vice versa. To find these set of values, the map of the "spin squared" values in terms of pds and Δ is obtained. It is shown in Fig.3.8 which has two distinct spin areas corresponding to low spin and high spin states. Each point in the red or high spin area gives the corresponding high spin pds and Δ values. Therefore, for any given value of pds and Δ the spin state can be predicted by the map.

$tpp = 0.8,\ pds = -1.9,\ 10Dq = 0.5,\ U_{dd} = 7.5,\ U_{pd} = 9,\ \ \Delta = 3.75\ \ Dist = 0\ eV$

$N_{e_g} = 1.618,\ N_{t_{2g}} = 5.958, N_d = 7.575$

$\alpha_1^2 = 0.485,\ \alpha_2^2 = 0.455,\ \alpha_3^2 = 0.058,\ \alpha_4^2 = 0.001$

$S^2 = 0.993$

Figure 3.3:   XAS spectra just before the spin state transition

$tpp = 0.8,\ pds = -1.9,\ 10Dq = 0.5,\ U_{dd} = 7.5,\ U_{pd} = 9,\ \ \Delta = 3.80,\ \ \ Dist = 0\ eV$

$N_{e_g} = 2.386,\ N_{t_{2g}} = 4.993, N_d = 7.379$

$\alpha_1^2 = 0.646,\ \alpha_2^2 = 0.329,\ \alpha_3^2 = 0.025,\ \alpha_4^2 = 0.000$

$S^2 = 3.099$

Figure 3.4:   XAS spectra just after the spin state transition

$tpp = 0.8$ $pds = -1.65$ $10Dq = 0.5$, $U_{dd} = 7.5$, $U_{pd} = 9$, $\Delta = 2.5$, $Dist = 0$ eV

$N_{e_g} = 1.673$, $N_{t_{2g}} = 5.960$, $N_d = 7.633$

$\alpha_1^2 = 0.434$, $\alpha_2^2 = 0.499$, $\alpha_3^2 = 0.065$, $\alpha_4^2 = 0.001$
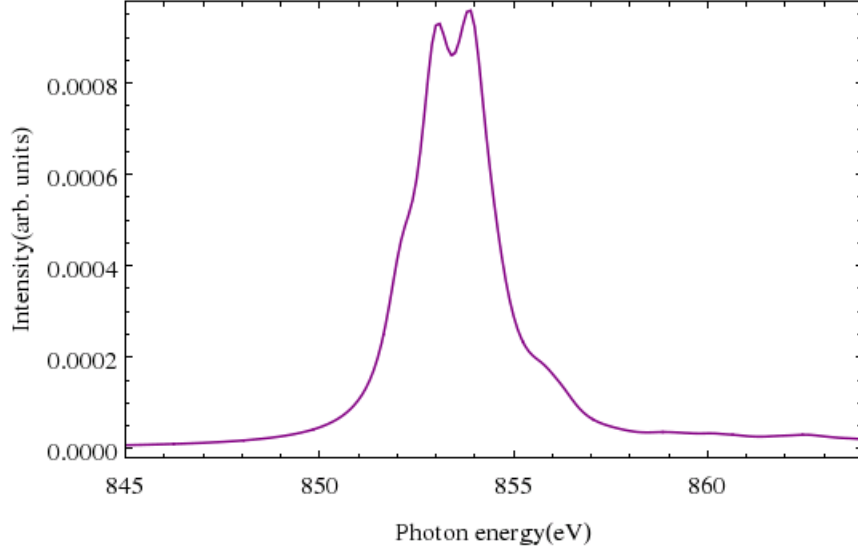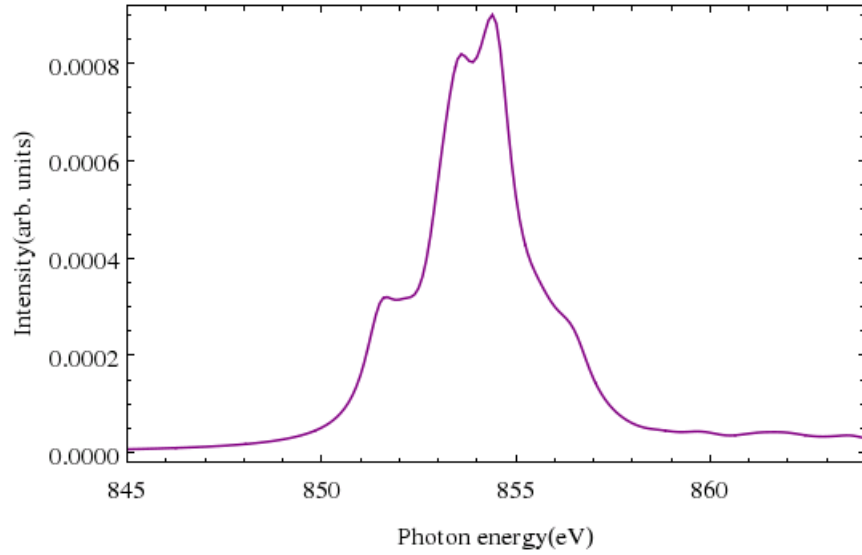
$S^2 = 1.046$
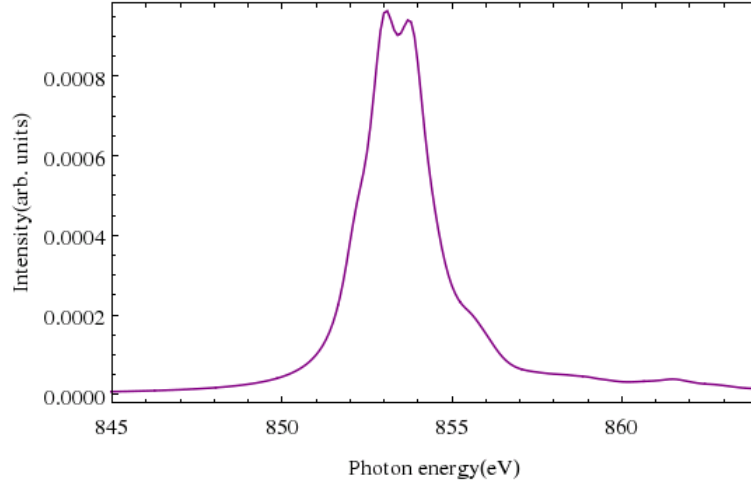
Figure 3.5:   XAS spectra just before the spin state transition

$tpp = 0.8$, $pds = -1.60$, $10Dq = 0.5$, $U_{dd} = 7.5$, $U_{pd} = 9$, $\Delta = 2.5$, $Dist = 0$ eV

$N_{e_g} = 1.673$, $N_{t_{2g}} = 5.960$, $N_d = 7.633$

$\alpha_1^2 = 0.434$, $\alpha_2^2 = 0.499$, $\alpha_3^2 = 0.065$, $\alpha_4^2 = 0.001$

$S^2 = 3.049$

Figure 3.6:   XAS spectra just after the spin state transition

TEY signal of pure CoO taken for different samples and in different beamlines: CLS Sep 2012, Berline Dec 2012 and from Change et al paper.

Figure 3.7:   High spin CoO XAS spectra from experiment
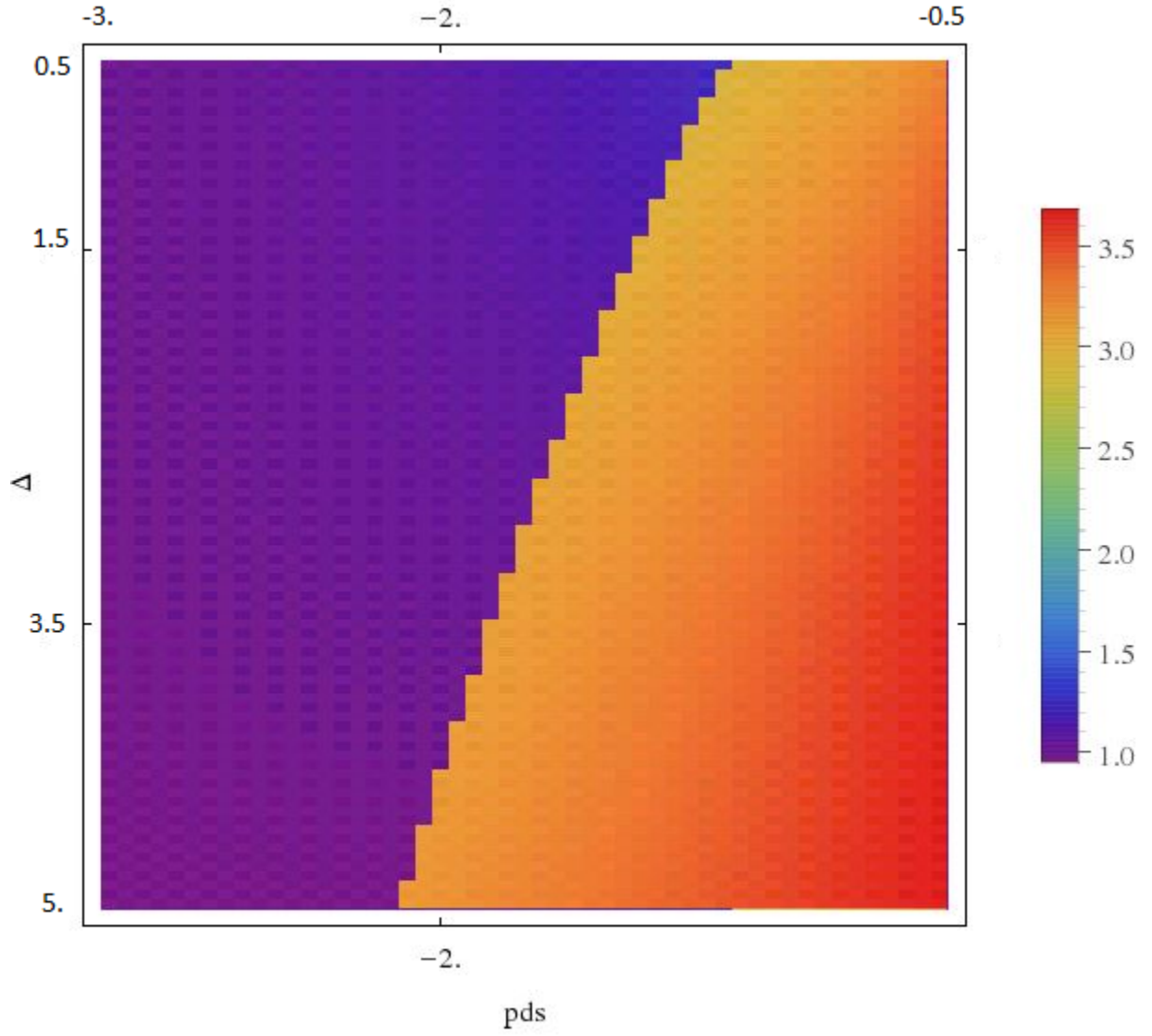
Figure 3.8: Map of the spin values versus Δ and *pds* showing the low spin to high spin transition

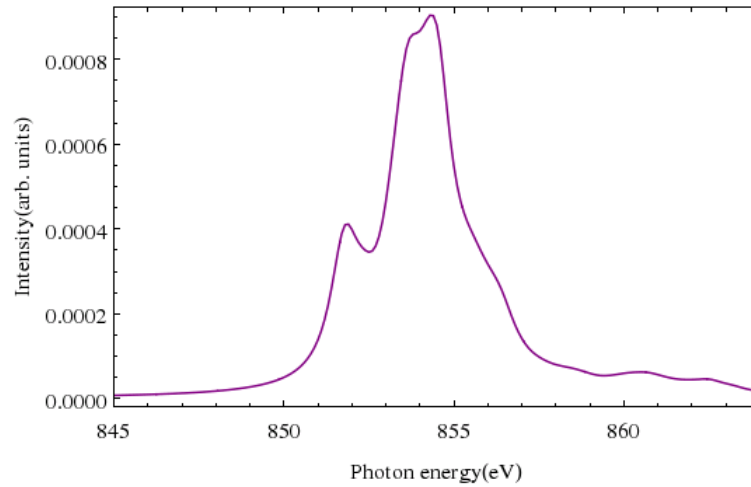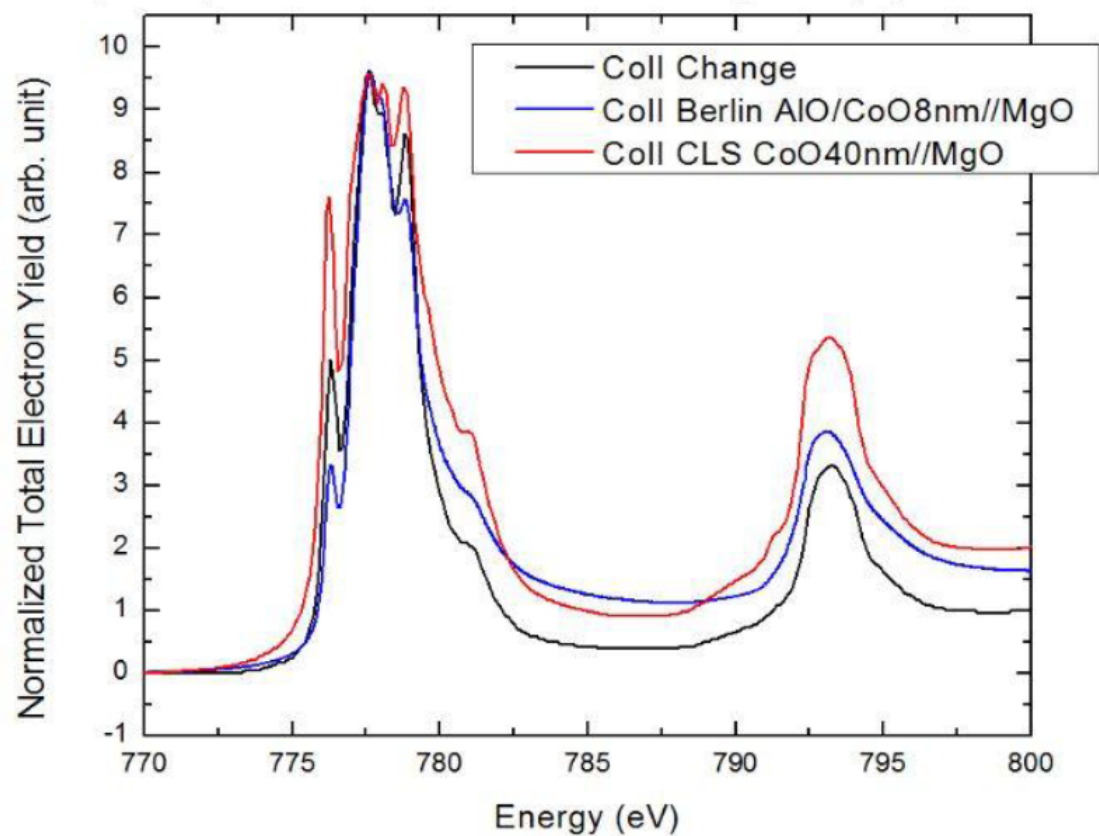Another interesting feature regarding spin state transition is illustrated in the ground state energy level diagrams. The first fifty ground state eigenvalues versus *pds* and Δ are shown respectively in Fig.3.9 and 3.10 It can be seen that in both cases exactly at the spin state transition critical values, the first two energy levels are crossed. It basically says that while before the low to high spin transition, the lowest ground state energy is corresponding to the spin half state and the first excited one is corresponding to the spin $\frac{3}{2}$, after the transition the situation goes the other way around making the spin $\frac{3}{2}$ state the new ground state and the first excited state the spin half state.
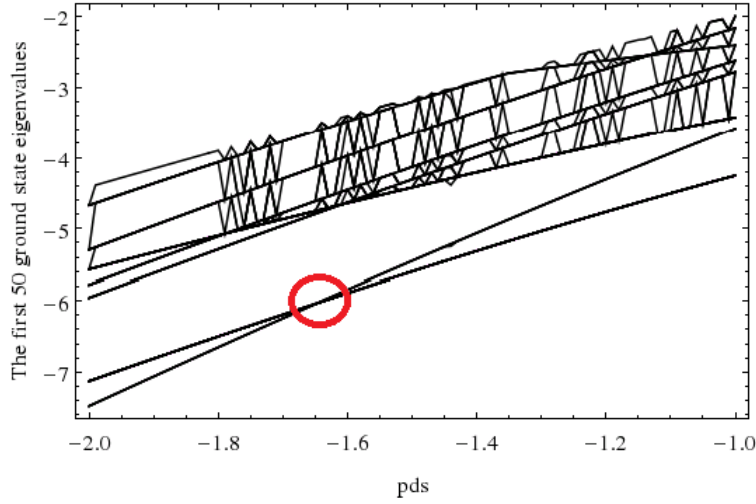
Figure 3.9:   Energy level diagram versus pds
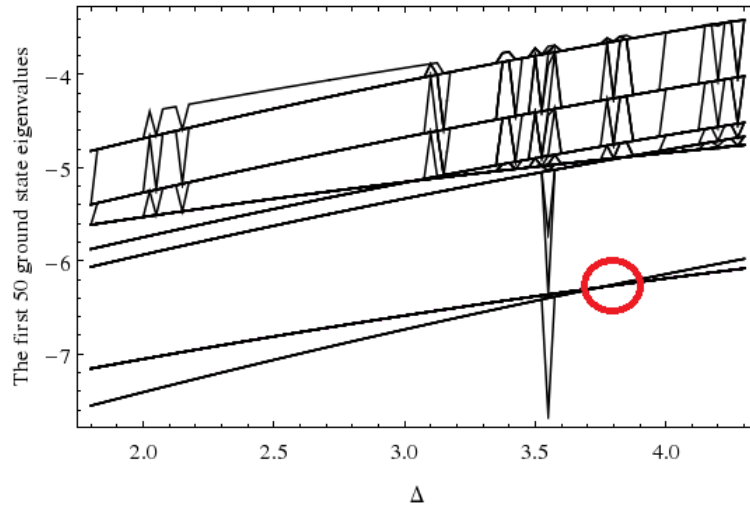
Figure 3.10:   Energy level diagram versus charge transfer energy

However by doing the MLFT cluster calculation in a nickelate single cluster, some interesting

features such as the spin transition have been obtained, the final XAS result does not match to the experiment very well unlike the result for NiO, MnO or $SrTiO_3$. [8] Therefore we can not really rely on the values have obtained by fitting the above calculations to the XAS experiment. In the next chapter the same method is used to obtain RIXS spectra in order to understand the material and the employed theory more deeply.

Chapter 4

RIXS Calculations

4.1 Seeking the Best Agreement with Experiment

Here again we need an experimental reference which is RIXS results from Geneva on $NdNO_3$. In NNO, nickel is again 3+ and since we are treating a single cluster of nickelate, it should not be very different than the Nickel 3+ in PNO [19]. The spectra is shown in Fig.4.1

As explained in the previous chapter, here photon excites an electron from the $2p$ to the $3d$ shell, then an electron decays into the core hole and a photon comes out. The first peak corresponds to the elastic process where no energy is lost and the second electron decays from the same level of energy as the excited one.

Fig. 4.1 shows the experimental RIXS spectra at different resonance energies about the XAS L_3 peak for two different temperatures. RIXS can be conducted by employing light with two different polarizations as here in Fig.4.1 LV and LH denote vertical and horizontal light polarizations.

The geometry of this experiment is illustrated in Fig.4.2. It clarifies what the different light polarizations imply here.

From Fig. 4.2 the following vectors' orientations are concluded. The calculations have also done with respect to the experiment geometry.

$$K_{in} = \{\cos 15°, 0, \sin 15°\}$$

$$K_{out} = \{\cos 65°, 0, \sin°\}$$

$$\sigma_{in} = LV_{in} = \{0, 1, 0\}$$

$$\sigma_{out} = LV_{out} = \{0, 1, 0\}$$

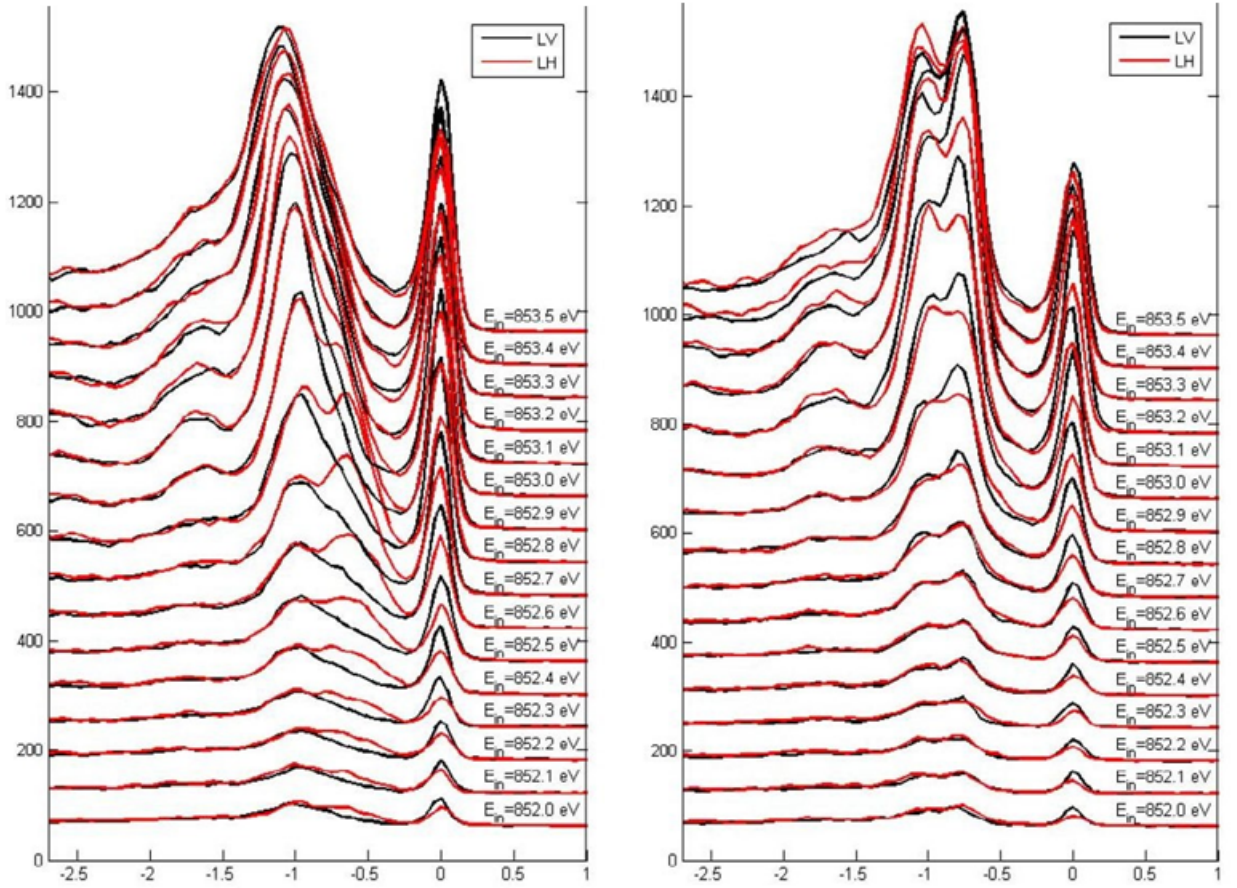$$\pi_{in} = LH_{in} = \{-\sin 15°, 0, \cos 15°\}$$

$$\pi_{out} = \{-\sin 65°, 0, \cos 65°\}$$

Figure 4.1: The experimental RIXS spectra form Geneva at T=300K in the left and at T=15K in the right.

To calculate these kind of spectra in principle three basis sets and three Hamiltonians are needed, corresponding to the initial, intermediate and final states. But in this case initial and final basis sets are the same and the intermediate state has the same basis set as the XAS state.

A very simple sketch of this second order process for a d^7 system is illustrated in Fig.4.3 It only shows one of the $d - d$ excitation possibilities, which actually should be the first one.

For each incoming polarization, the RIXS spectra are obtained by adding the both possible outgoing light polarizations. Now by choosing the resonance energy from XAS spectra, the corresponding RIXS spectrum can be calculated.

To be able to compare the results with experiment, the same resonance energies near the L_3 peak, on the left shoulder, are chosen. The energies are relative, they are shifted to match the experiment as much as possible for convenience. The other parameters such as hopping

Figure 4.2: RIXS experimental geometry
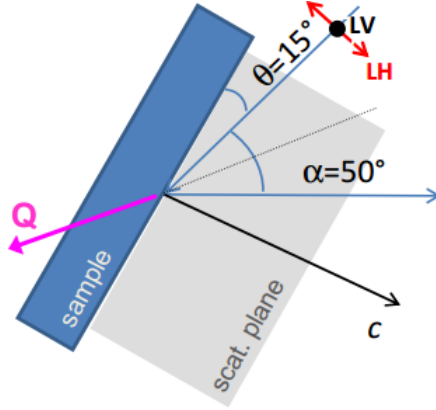
- **θ** or incidence angle = 15° (corresponding to 255° in the manipulator units)
- **α** or back-scattering angle = 50°
- **LV** or **σ** or out-of-plane* polarization: parallel to the *ab* crystal plane
- **LH** or **π** or in-plane* polarization: almost parallel to the *c* crystal axis
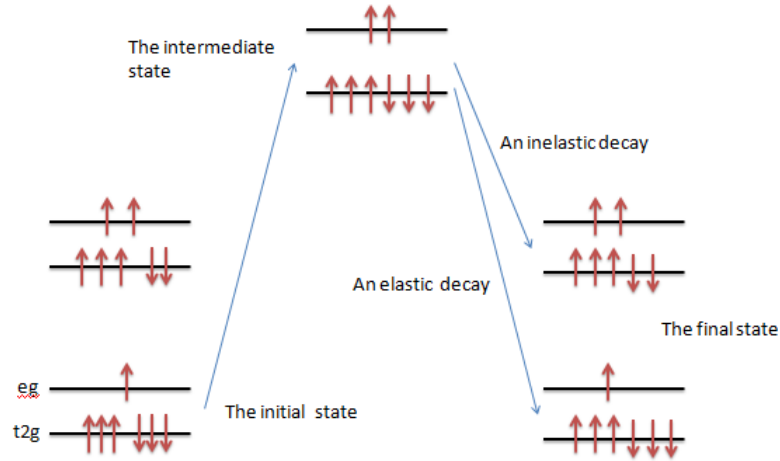
Figure 4.3: A schematic sketch of the $d-d$ excitations in a d^7 low spin system.

integrals, charge transfer energy and $10Dq$ are set as the final values in the second chapter obtained by matching to the XAS from experiment . The intermediate state(XAS) broadening and RIXS spectra broadening are set to be 0.2 and 0.3 eV respectively. The resonant energies are shown on the XAS spectra in Fig.4.5 and the corresponding RIXS results are presented in Fig. 4.4

The room temperature RIXS spectra in Fig. 4.1 shows a continuum behaviour in its $d-d$ like excitations. By looking at the phase transition diagram for NdNo in chapter one,1.1 it can

be seen that at 300°, the system is in its metallic phase. So there is no gap to jump and make an excitation. That is why the spectra basically says that for any given energy an excitation can occur. Our calculations does not include metallic phase. It models the insulting behaviour as discussed in the previous chapters.

In the low temperature RIXS results, the lowest excitations happen at about 0.8 eV. For now, we assume it is corresponding to the lowest $d - d$ excitation and no excitation peak is lost in the elastic peak broadening. On the other hand, in the calculated spectra the first observable excitation peak happens at about 1.4 eV as shown in Fig. 4.4 To understand which excitation this peak corresponds to, the first eigen-energies of the system are calculated. They are presented in table 4.1 The peaks' energies in the RIXS spectra are basically the relative eigen-energies of the system. The magnon and phonon excitations are not considered here. table 4.1 suggests that in fact the first $d - d$ excitation peak in our calculation happens at a too *low* energy (0.25 eV) and can not be observed in our spectra. In order not to loose it, the RIXS broadening is decreased to 0.2 eV. The results at the resonant energies of 853 and 853.2 eV are presented in Fig.4.6 and the relative eigen-energies are also shown on them with the vertical lines. The other spectra at the other incident energies are presented in the appendix.

Figure 4.4: Calculated RIXS spectra for the following values: $tpp = 0.8$, $pds = -1.9$, $\Delta = 2.5$, $10Dq = 0.5$, $U_{dd} = 7.5$, $U_{pd} = 9$ eV and RIXS broadening of 0.3 eV

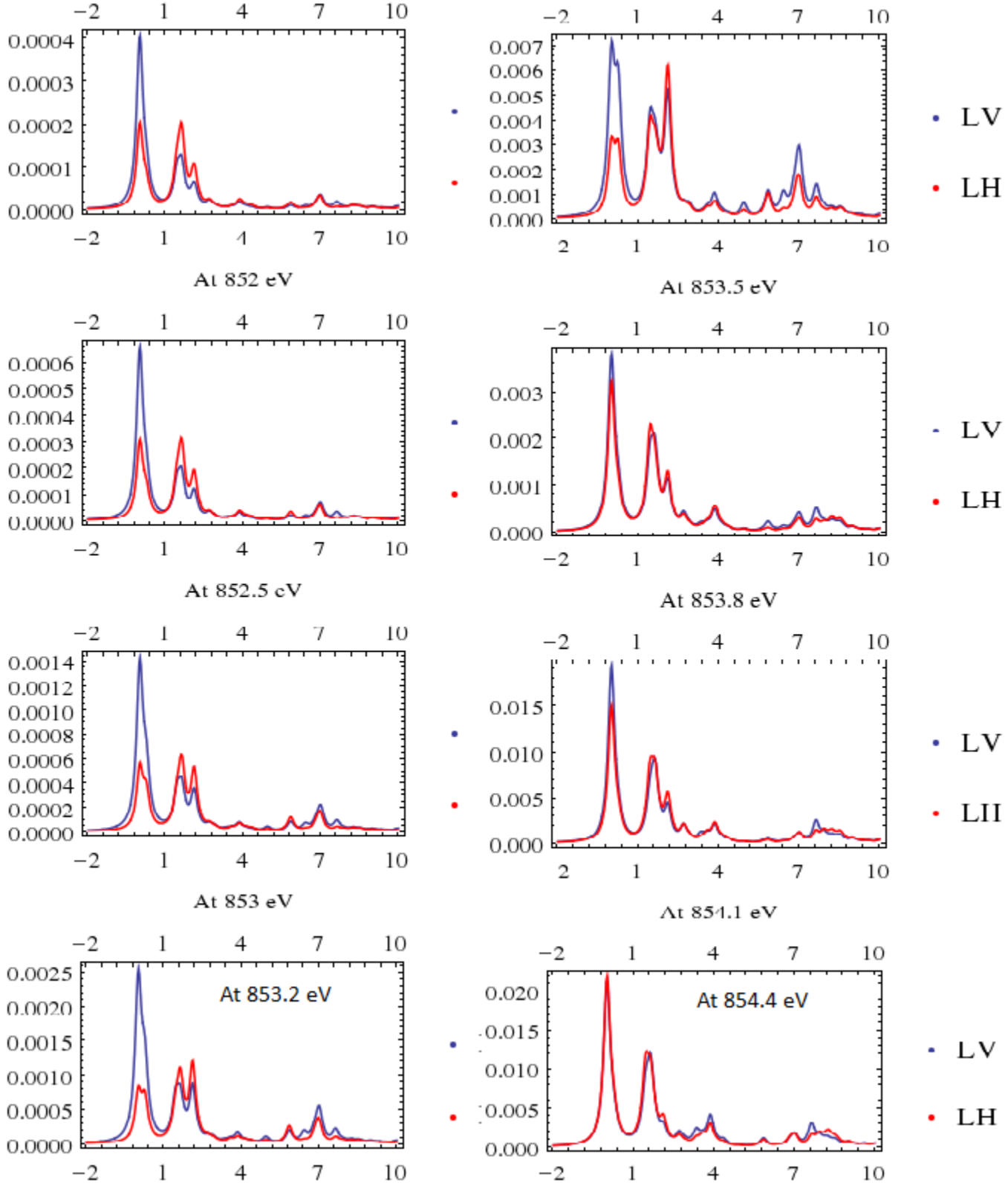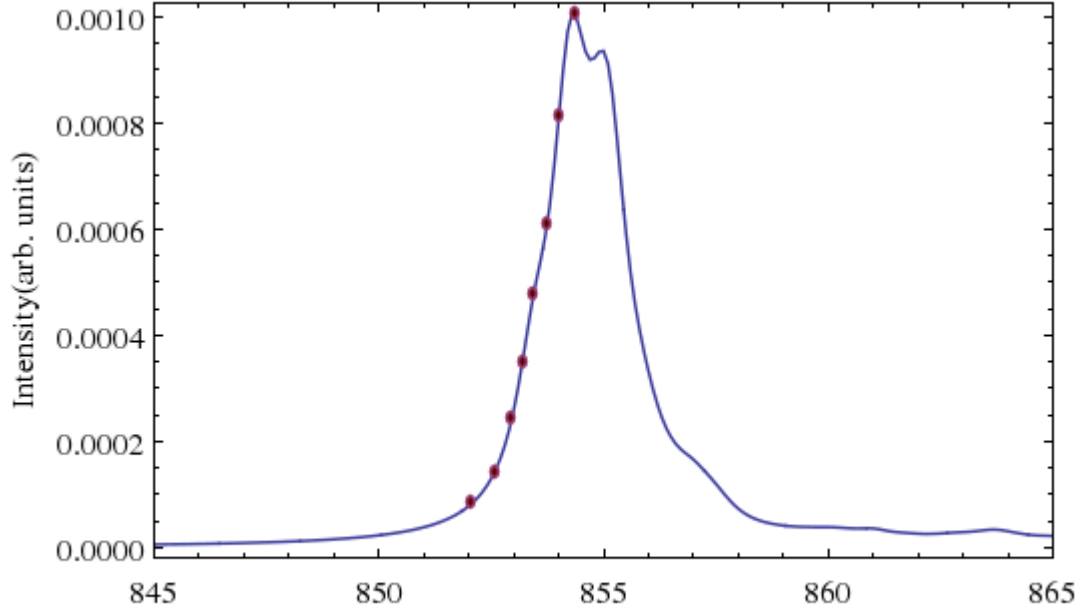Figure 4.5: The resonant energies taken for the RIXS calculations, at 852 ,852.5, 853, 853.2, 853.5, 853.8, 854.1, 854.4 eV with the following values $tpp = 0.8$, $pds = -1.9$, $\Delta = 2.5$, $10Dq = 0.5$, $U_{dd} = 7.5$, $U_{pd} = 9$ eV and RIXS broadening of 0.2 eV

Index	Energy	Relative Energy
1	-7.05965	0.
2	-7.05965	0
3	-7.05965	0
4	-7.05965	0
5	-6.68067	0.378976
6	-6.68067	0.378976
7	-6.68067	0.378976
8	-6.68067	0.378976
9	-6.68067	0.378976
10	-6.68067	0.378976
11	-6.68067	0.378976
12	-6.68067	0.378976
13	-6.68067	0.378976
14	-6.68067	0.378976
15	-6.68067	0.378976
16	-6.68067	0.378976
17	-5.50959	1.55006
18	-5.50959	1.55006
19	-5.50959	1.55006
20	-5.50959	1.55006
21	-5.50959	1.55006
22	-5.50959	1.55006
23	-5.30824	1.75141
24	-5.30824	1.75141
25	-5.30824	1.75141

Table 4.1: The first 25 eigen-energies of the system with $\Delta = 2.5eV$.

At 853 eV

At 853.2 eV

Figure 4.6: Calculated RIXS spectra with the following parameters: $\Delta = 2.5$, $tpp = 0.8$, $pds = -1.9$, $10Dq = 0.5$, $U_{dd} = 7.5$, $U_{pd} = 9$ eV and RIXS broadening of 0.2 eV. The vertical axis is the intensity in an arbitrary unit and the horizontal axis is the energy loss in eV.

This inconsistency between the experiment and the calculation can be addressed by tuning the charge transfer energy (Δ) and hopping integral (pds). The splitting enegy which determines the energy at which the first $d - d$ excitation happens, is inversely proportional to the charge transfer energy. Therefore, to increase this energy from about 0.25 to about 0.8 eV we have to decrease Δ dramatically. By calculating the eigen-energies of the system with the different smaller Δs, for $\Delta = 0.5 eV$, the splitting of 0.67 eV is obtained which is almost equal to the splitting energy in the experiment.

The XAS spectra with this Δ and the given resonant energies are shown in Fig.4.7 The corresponding RIXS spectra at the two of these energies are also presented in Fig. 4.8, the other ones are shown in the appendix.

Figure 4.7: The resonant energies taken for the RIXS calculations, at 851.2 ,851.6, 852, 852.3, 852.5, 852.7, 852.9, 853.4, 853.6 eV with the following values $\Delta = 0.5$, $tpp = 0.8$, $pds = -1.9$, $10Dq = 0.5$, $U_{dd} = 7.5$, $U_{pd} = 9$ eV
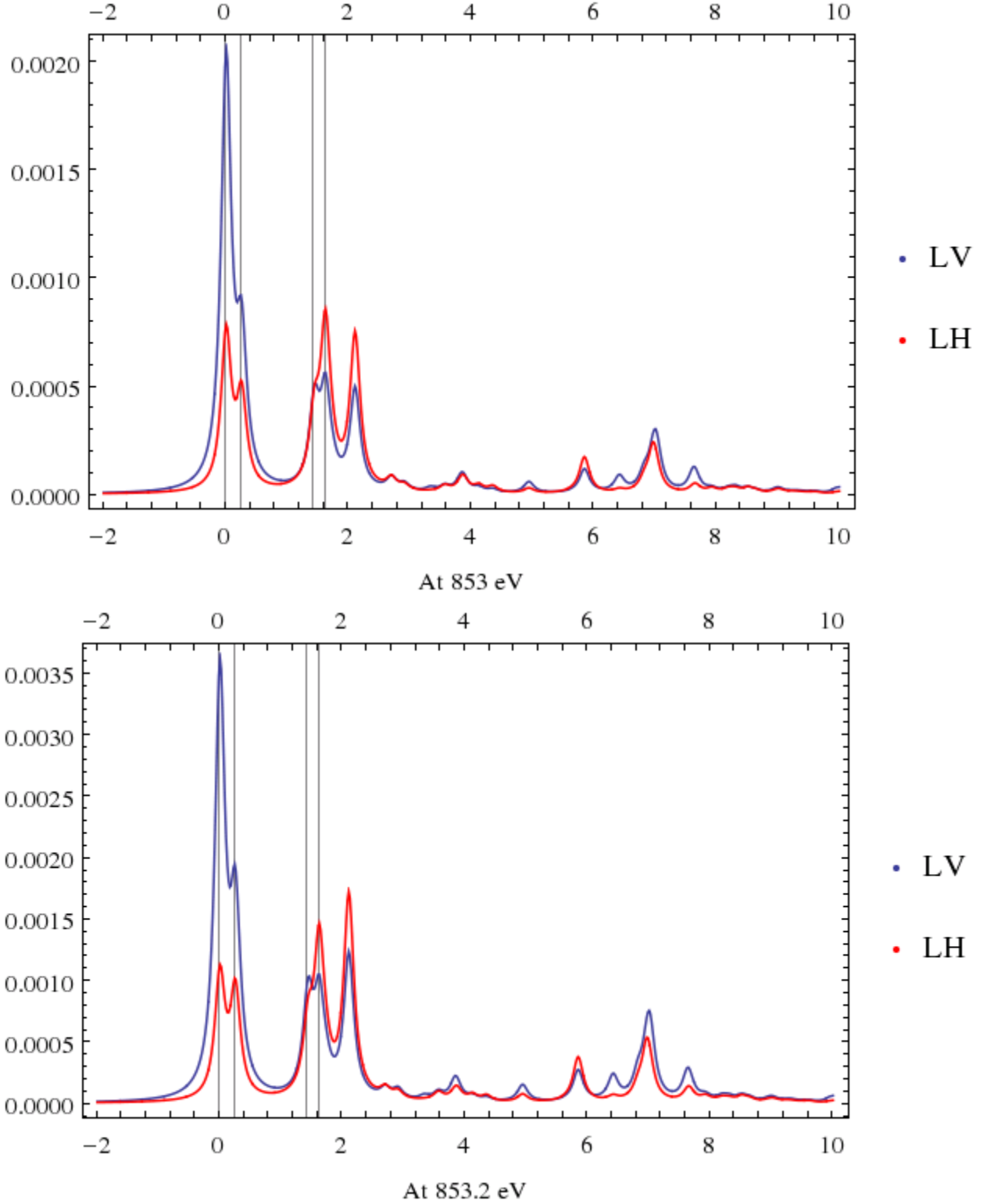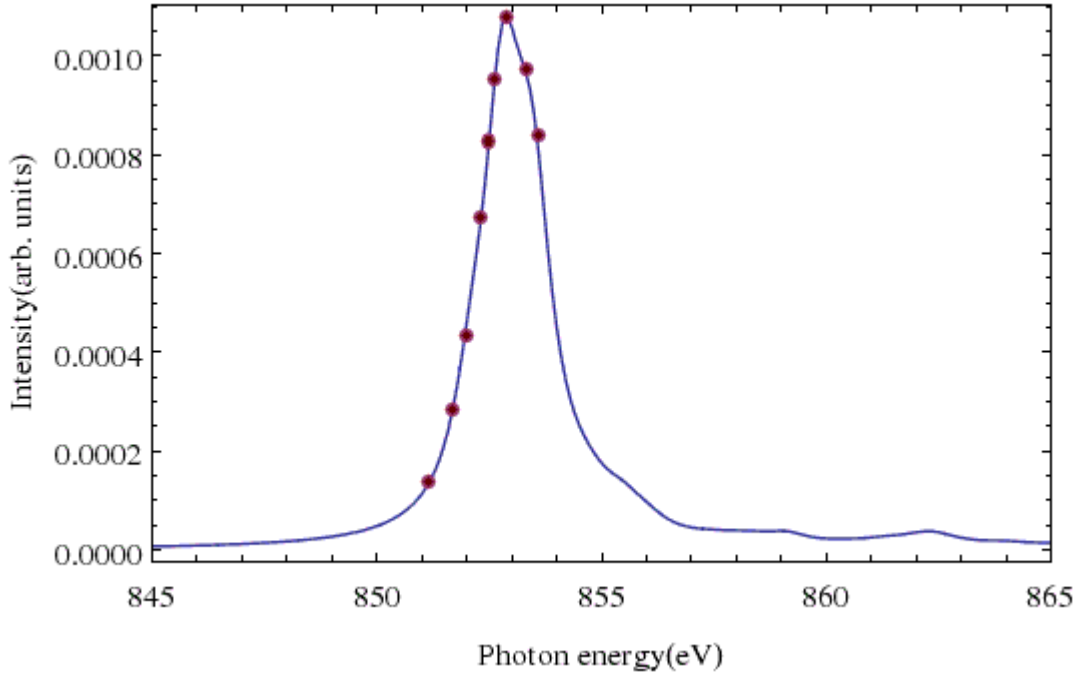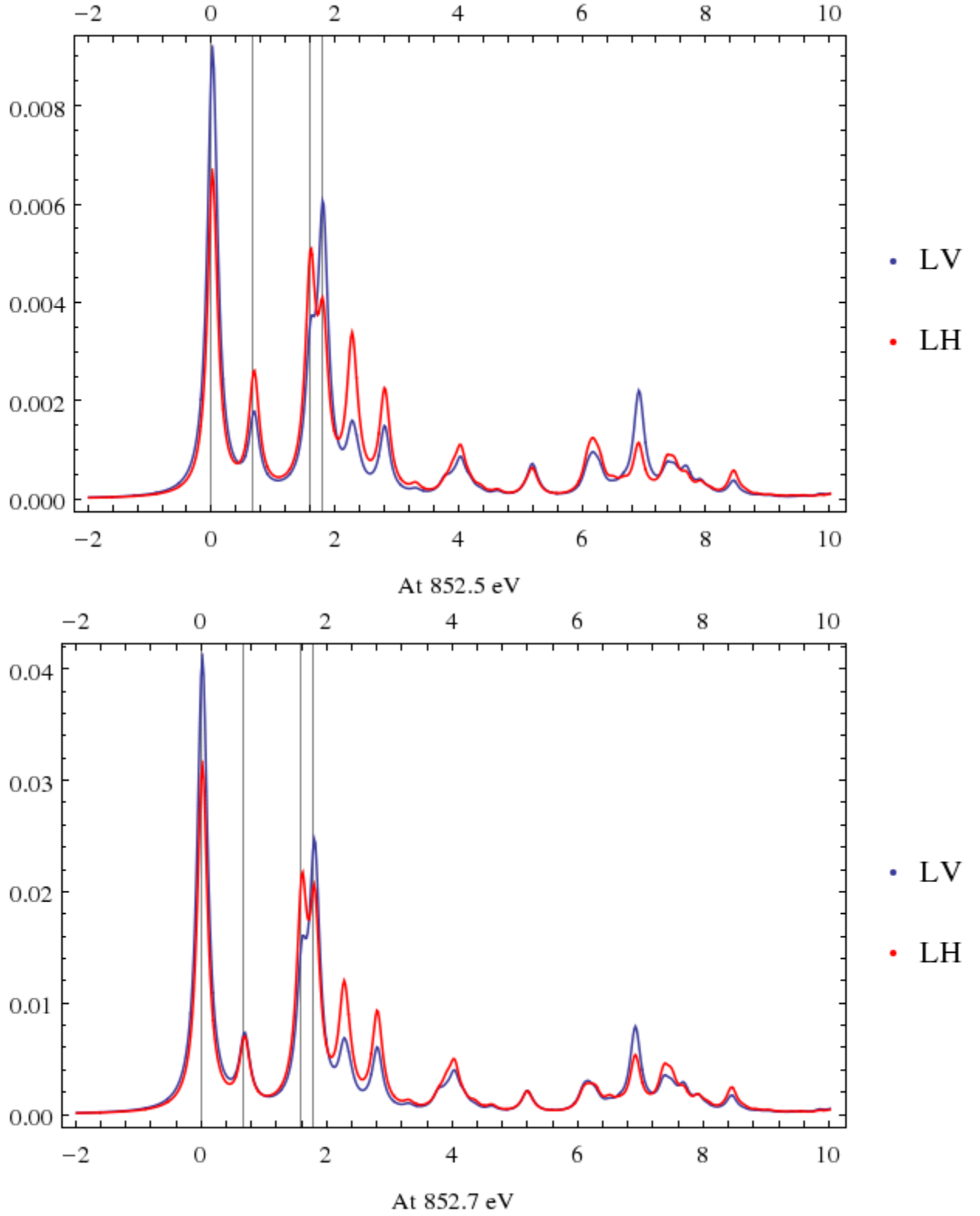
At 852.5 eV

At 852.7 eV

Figure 4.8: Calculated RIXS spectra with the following parameters: $\Delta = 0.5$, $tpp = 0.8$, $pds = -1.9$, $10Dq = 0.5$, $U_{dd} = 7.5$, $U_{pd} = 9$ eV

Index	Energy	Relative Energy
1	-8.57345	0.
2	-8.57345	0
3	-8.57345	0
4	-8.57345	0
5	-7.89973	0.673718
6	-7.89973	0.673718
7	-7.89973	0.673718
8	-7.89973	0.673718
9	-7.89973	0.673718
10	-7.89973	0.673718
11	-7.89973	0.673718
12	-7.89973	0.673718
13	-7.89973	0.673718
14	-7.89973	0.673718
15	-7.89973	0.673718
16	-7.89973	0.673718
17	-6.98748	1.58596
18	-6.98748	1.58596
19	-6.98748	1.58596
20	-6.98748	1.58596
21	-6.98748	1.58596
22	-6.98748	1.58596
23	-6.78415	1.78929
24	-6.78415	1.78929
25	-6.78415	1.78929

Table 4.2: The first 25 eigen-energies of the system with $\Delta = 0.5eV$.

What we have done so far is decreasing the charge transfer energy from 2.5 to 0.5 eV to increase the splitting or the first $d - d$ excitation energy to 0.67 eV in order to match the calculated RIXS to the experimental ones. Now the problem with the new RIXS spectra is the intensity ratios and the polarization dependence. To adjust the splitting energy by changing Δ, we had assumed that the first peak in the experiment is the one associated with the first to the second eigen-states. It might not be the case. The first inelastic peak in experiment has an intensity comparable to the elastic peak or even larger. It also has a double peak which shows polarization dependence at some resonant energies. They all are the characteristics of our second inelastic calculated peak. Therefore, it can be concluded that the first excitation in the experiment is also happening in a very low energy smaller than the experiment resolution (less

than 0.1 eV) and then the second inelastic excitation happened at bout one eV. By considering the relation between the charge transfer energy and the hopping integral and the splitting energy, and calculating the first eigen-energies for several cases, it has been obtained that for the values of $\Delta = 0.8$ and $pds = -1.4$, the best agreement can be obtained. Remember we have to consider the spin transition and not let the system make the transition to the high spin state. The allowed low spin Δ and pds values can be taken from the spin state transition map in the previous chapter. 3.8

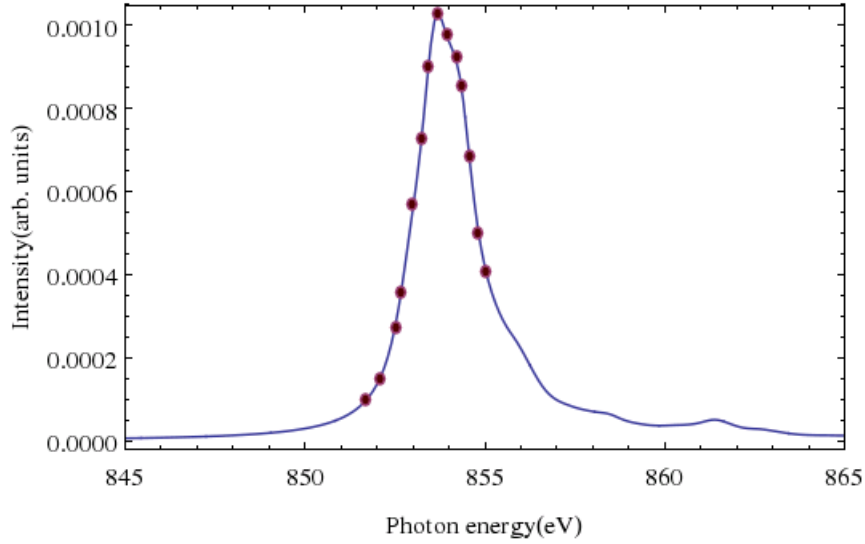The final RIXS results are also shown in figures 4.10 to 4.16.

Figure 4.9:   The resonant energies taken to calculate RIXS spectra with the following values $tpp = 0.8$, $pds = -1.4$, $\Delta = 0.8$, $10Dq = 0.4$, $U_{dd} = 7.5$, $U_{pd} = 9$ eV with energy shift of 865 eV

Index	Energy	Relative Energy
1	-6.07292	0.
2	-6.07292	0
3	-6.07292	0
4	-6.07292	0
5	-6.00779	0.0651309
6	-6.00779	0.0651309
7	-6.00779	0.0651309
8	-6.00779	0.0651309
9	-6.00779	0.0651309
10	-6.00779	0.0651309
11	-6.00779	0.0651309
12	-6.00779	0.0651309
13	-6.00779	0.0651309
14	-6.00779	0.0651309
15	-6.00779	0.0651309
16	-6.00779	0.0651309
17	-4.9985	1.07442
18	-4.9985	1.07442
19	-4.9985	1.07442
20	-4.9985	1.07442
21	-4.9985	1.07442
22	-4.9985	1.07442
23	-4.84256	1.23036
24	-4.84256	1.23036
25	-4.84256	1.23036

Table 4.3: The first relative eigen-energies of the system with the following values: $tpp = 0.8$, $pds = -1.4$, $\Delta = 0.8$, $10Dq = 0.4$, $U_{dd} = 7.5$, $U_{pd} = 9$ eV
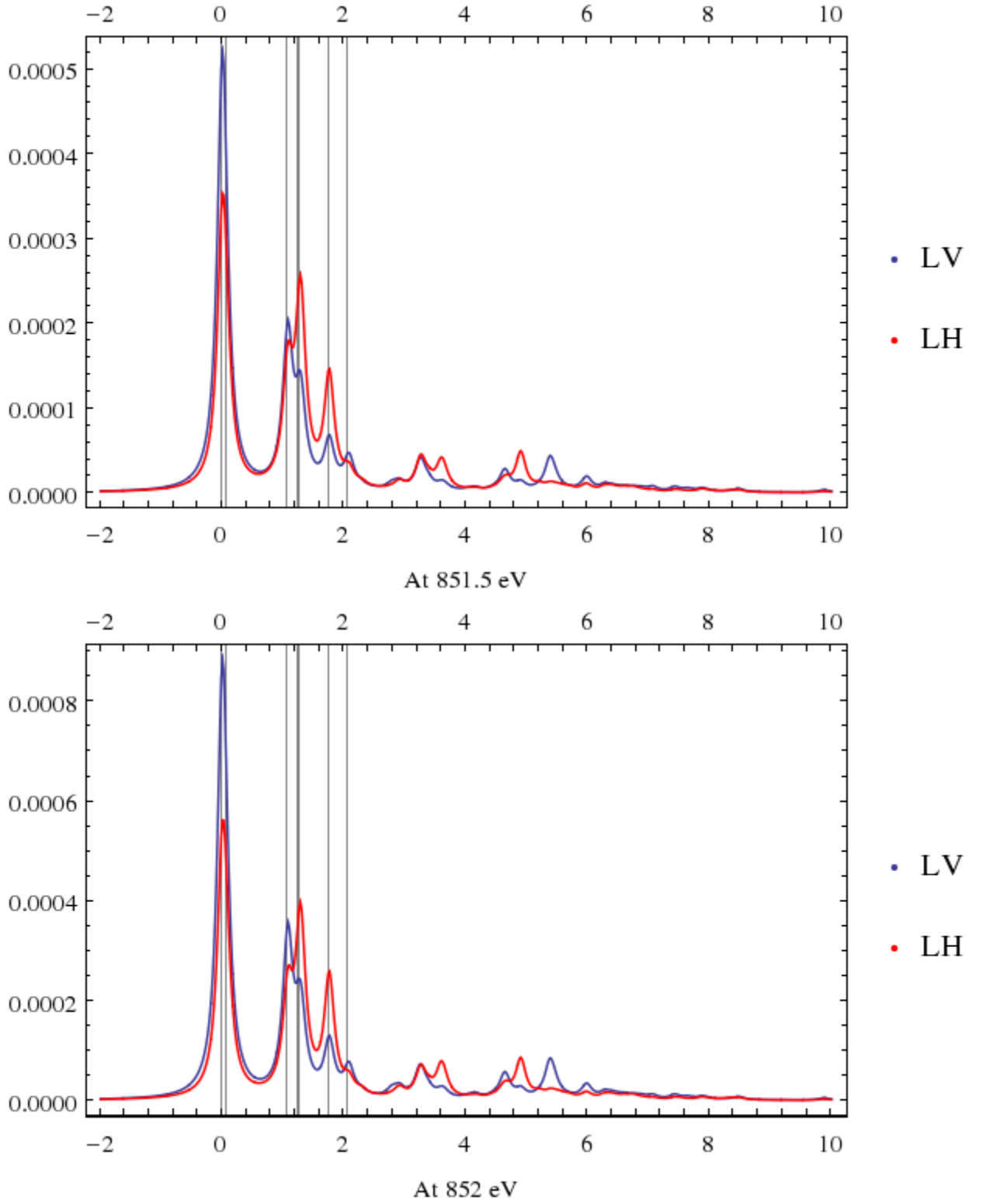
Figure 4.10: Calculated RIXS spectra with the following parameters: $\Delta = 0.8$, $tpp = 0.8$, $pds = -1.4$, $10Dq = 0.4$, $U_{dd} = 7.5$, $U_{pd} = 9$ eV
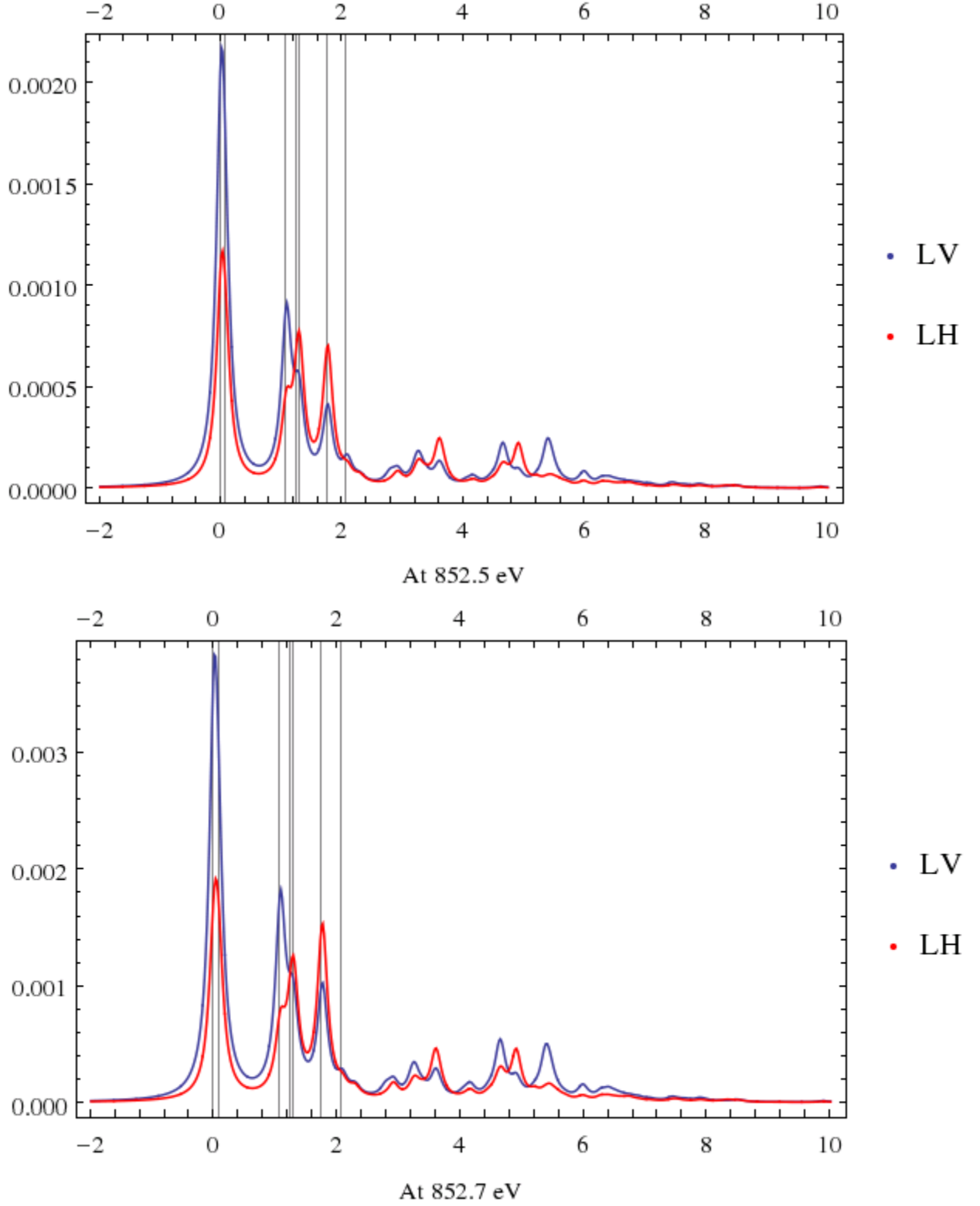
Figure 4.11: Calculated RIXS spectra with the following parameters: $\Delta = 0.8$, $tpp = 0.8$, $pds = -1.4$, $10Dq = 0.4$, $U_{dd} = 7.5$, $U_{pd} = 9$ eV

Figure 4.12: Calculated RIXS spectra with the following parameters: $\Delta = 0.8$, $tpp = 0.8$, $pds = -1.4$, $10Dq = 0.4$, $U_{dd} = 7.5$, $U_{pd} = 9$
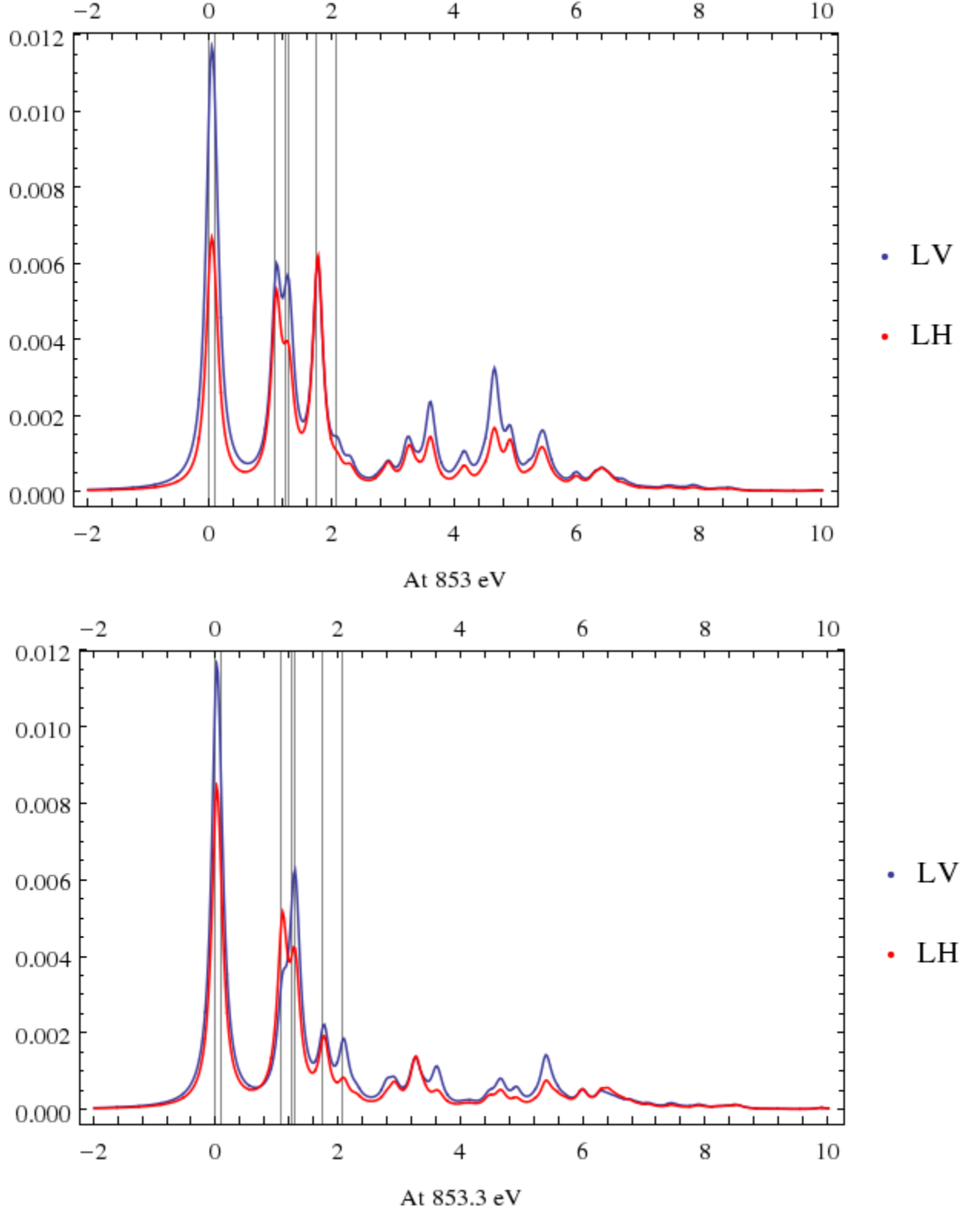
Figure 4.13: Calculated RIXS spectra with the following parameters: $\Delta = 0.8$, $tpp = 0.8$, $pds = -1.4$, $10Dq = 0.4$, $U_{dd} = 7.5$, $U_{pd} = 9$

Figure 4.14: Calculated RIXS spectra with the following parameters: $\Delta = 0.8$, $tpp = 0.8$, $pds = -1.4$, $10Dq = 0.4$, $U_{dd} = 7.5$, $U_{pd} = 9$
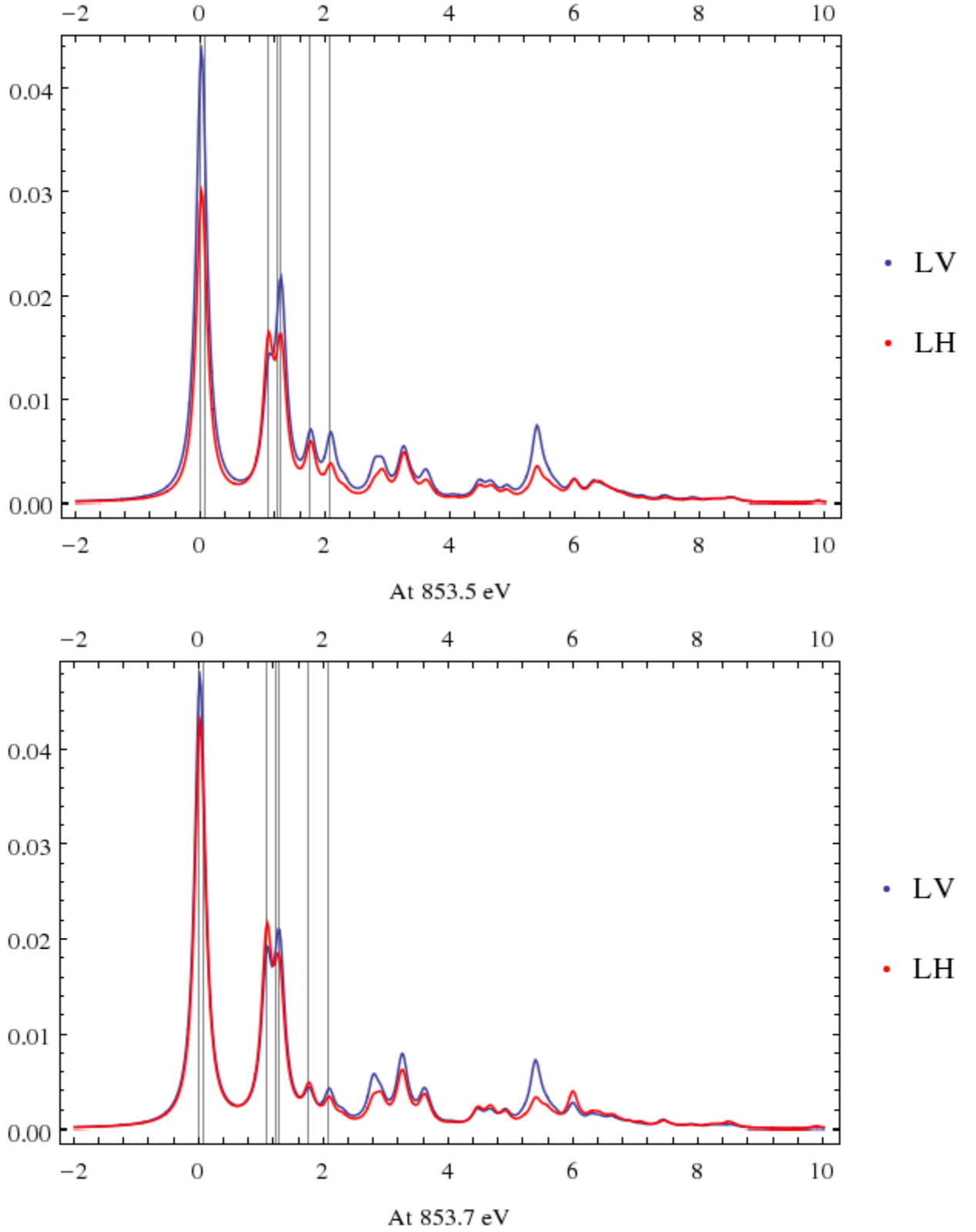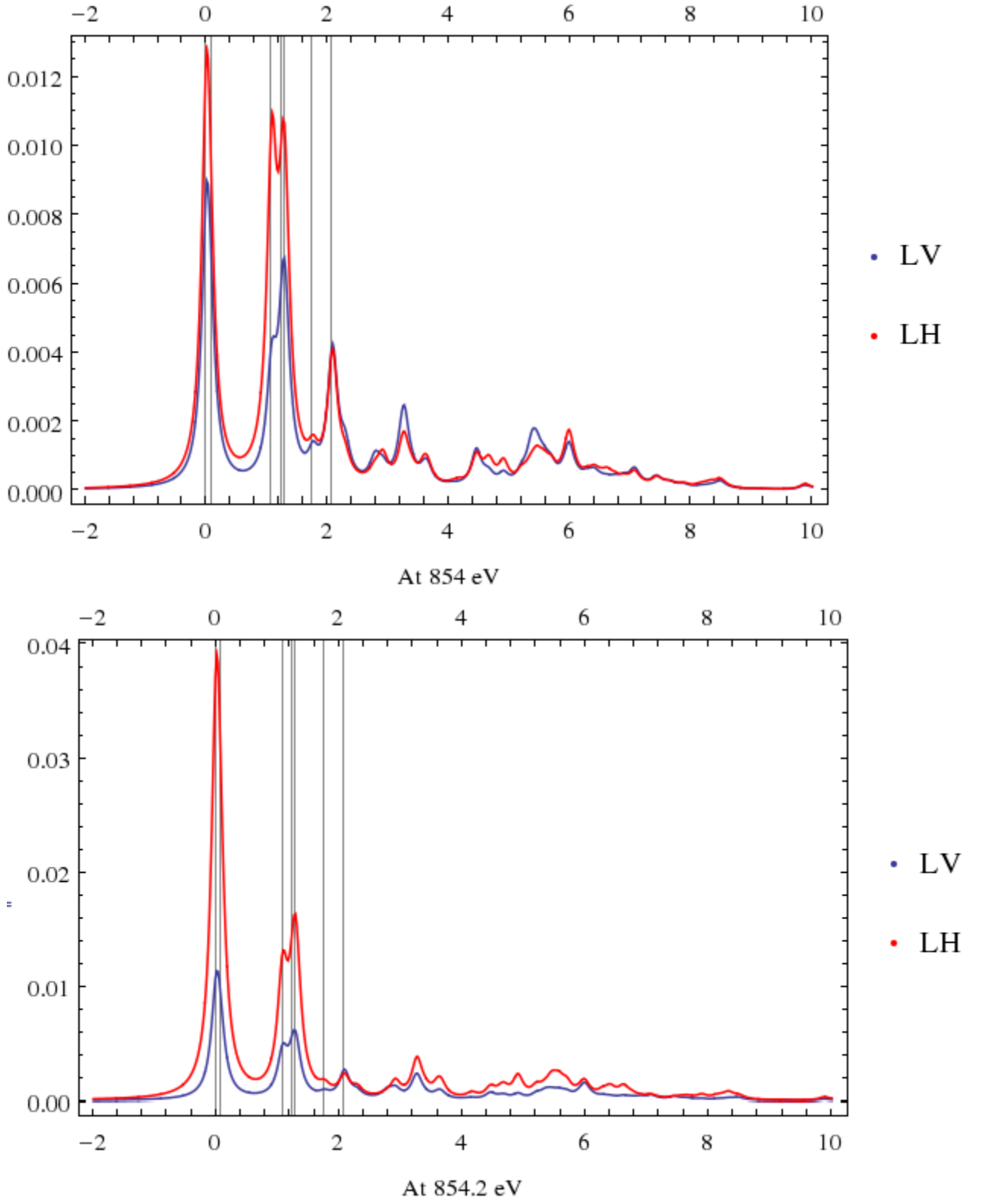
Figure 4.15: Calculated RIXS spectra with the following parameters: $\Delta = 0.8$, $tpp = 0.8$, $pds = -1.4$, $10Dq = 0.4$, $U_{dd} = 7.5$, $U_{pd} = 9$
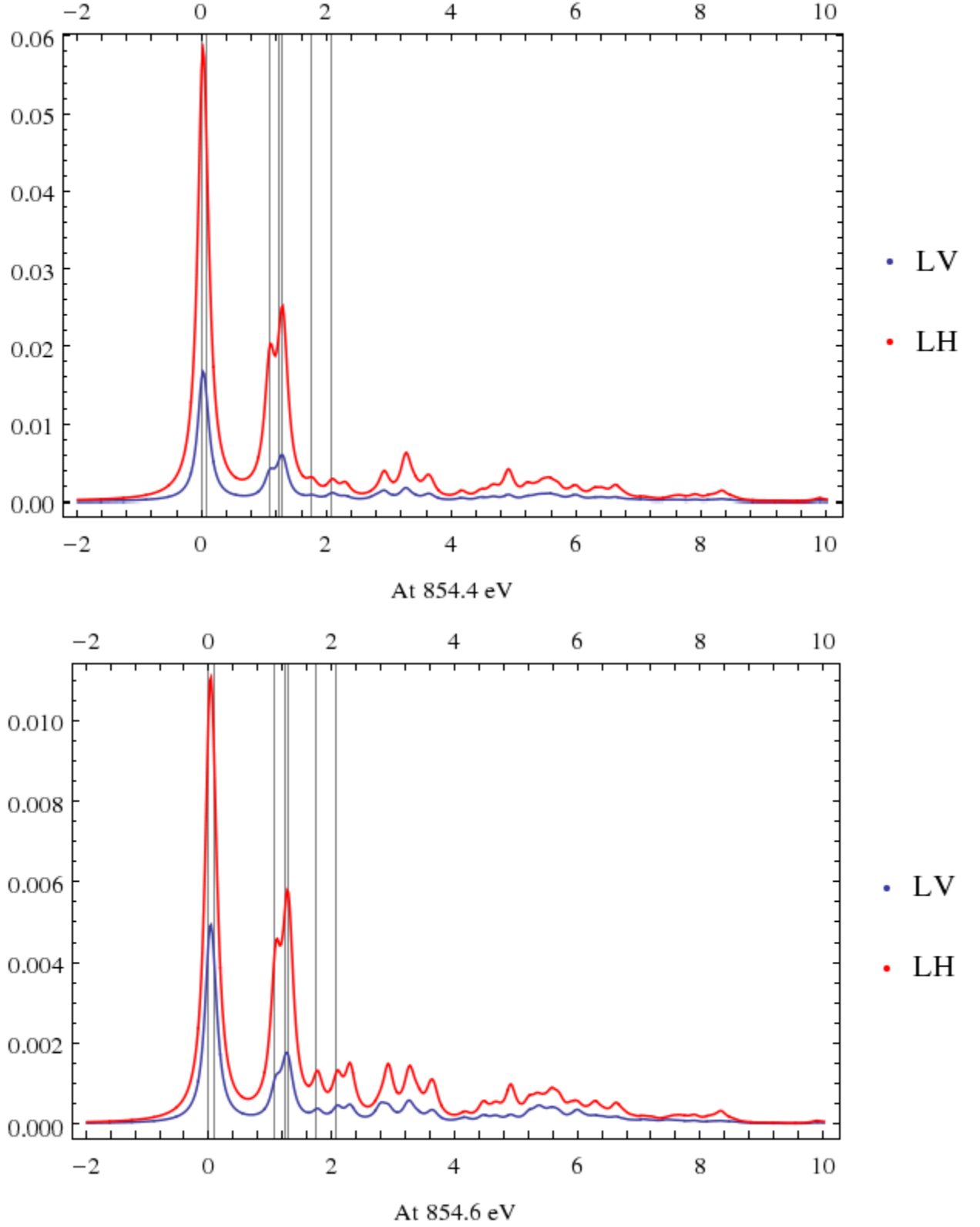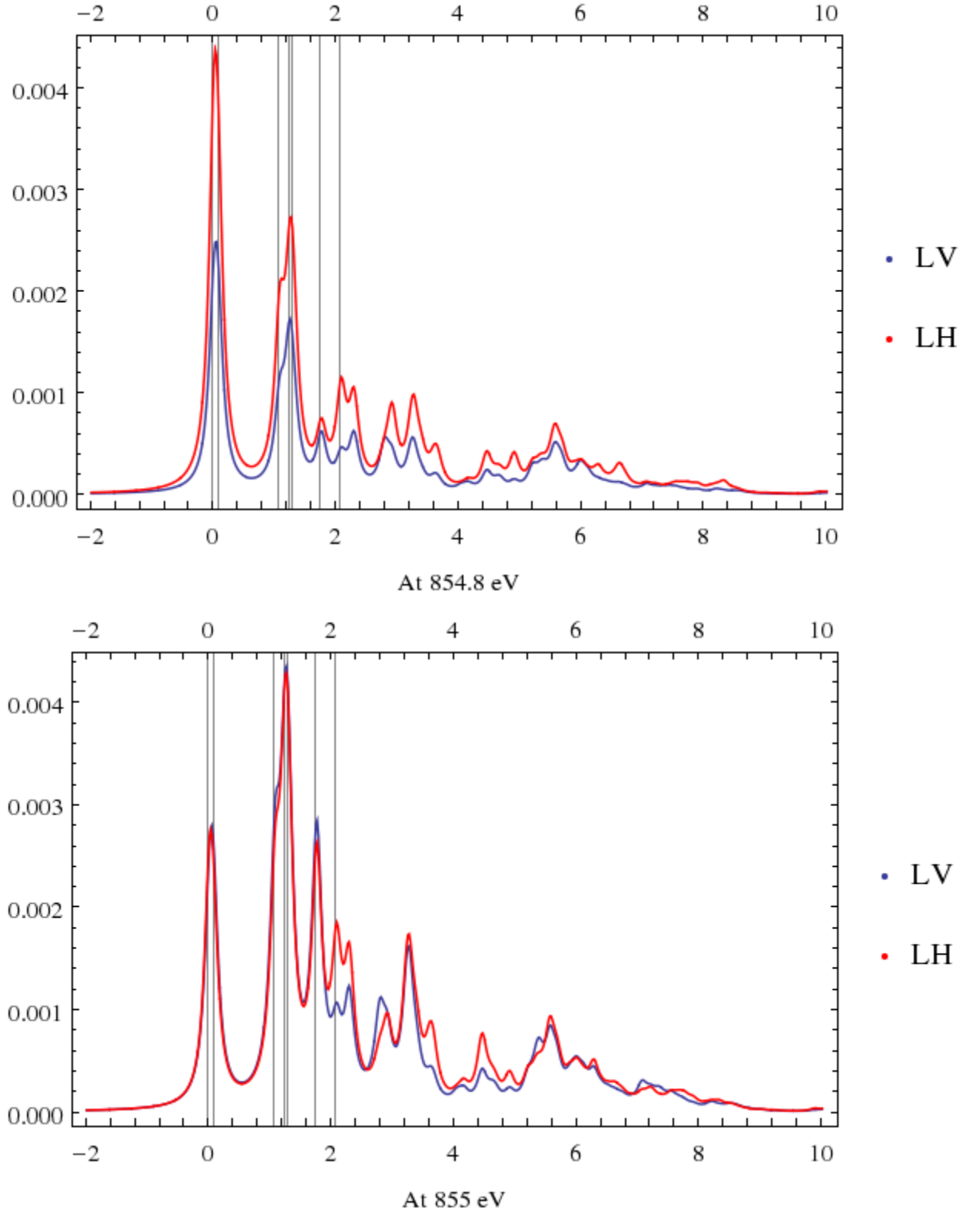
Figure 4.16: Calculated RIXS spectra with the following parameters: $\Delta = 0.8$, $tpp = 0.8$, $pds = -1.4$, $10Dq = 0.4$, $U_{dd} = 7.5$, $U_{pd} = 9$

Therefore, in order to match the elementary excitation energies in the experimental RIXS experiment with the calculation, we had to decrease charge transfer energy significantly and adjust the hopping integral and 10Dq a little bit. In terms of the polarization dependence in the calculated final RIXS, it has been seen that while there is a considerable polarization dependance at left side of the L_3 peak, there is no such a dependence at the right side, where the double peak should have existed. Considering the above points and the fact that even with the big Δ of 2.5 eV, the calculated and experimental XAS spectra presented huge differences, it can be concluded that the double peak in the L_3 may not be a result of multiplet structure but could have an origin beyond what can be included in a isolated cluster approach.

We should mention that the resonant inelastic x ray scattering spectra extended out to an energy region including the second peak of the L_3 XAS demonstrate a linear dispersion with incident energy after having passed through the first peak. This clearly demonstrates that the second peak has a very different origin and must involve a continuum state in which the excited electron in a state decoupled from the core hole and so does not participate in the decay to the core hole state. The resulting spectrum then is that of x ray fluorescence rather than resonant x ray inelastic scattering.

4.2 XAS Spectra with Parameters Driven from RIXS

The new fitted parameters from the previous section are $\Delta = 0.8$, $tpp = 0.8$, $pds = -1.4$, $10Dq = 0.4$, $U_{dd} = 7.5$, $U_{pd} = 9$, these new values will alter the calculated XAS spectra a lot. With this smaller Δ, the double peak in the L_3 peak will disappear. From the XAS calculation, we already know that in these type of calculations changing the charge transfer energy mostly changes the L_3 double peak intensity ratio, but from the RIXS results we concluded that maybe it is not the right approach to get the Δ from. This new calculated XAS is presented in Fig. 4.17 and the configuration contribution numbers and the number of electrons in the d shell are also calculated and presented. It can be seen that with these new values for the charge transfer energy and pds, $d^8 L^9$ configuration still has the largest contribution to the ground state and system is still in the low spin state.

$tpp = 0.8,\ pds = -1.4,\ 10Dq = 0.4,\ U_{dd} = 7.5,\ U_{pd} = 9,\ \Delta = 0.8,\ Distortion = 0.\ eV$

$N_{e_g} = 1.79,\ N_{t_{2g}} = 5.97, N_d = 7.76$

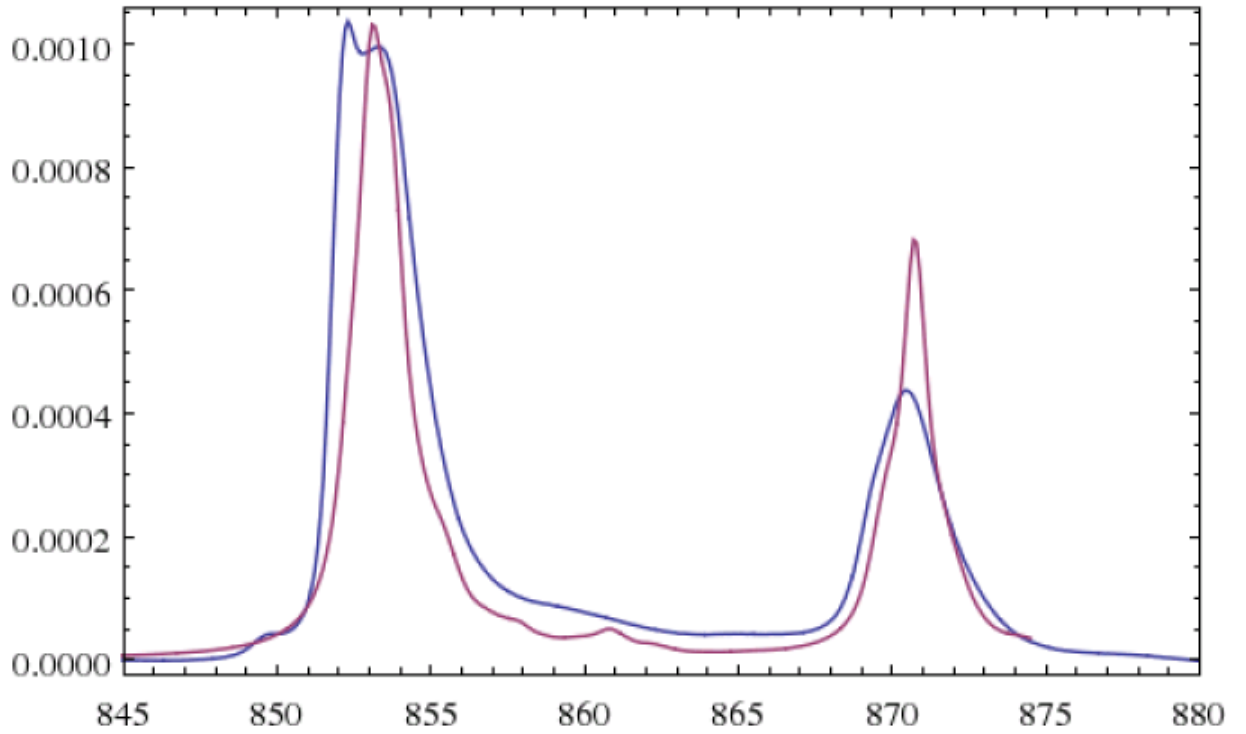$\alpha_1^2 = 0.34,\ \alpha_2^2 = 0.56,\ \alpha_3^2 = 0.09,\ \alpha_4^2 = 0.00$

$S^2 = 1.10$

Figure 4.17: Calculated XAS spectra with the following parameters: $\Delta = 0.8$, $tpp = 0.8$, $pds = -1.4, 10Dq = 0.4$, $U_{dd} = 7.5$, $U_{pd} = 9$ eV

Chapter 5

Conclusion

From the Zaanen-Sawatzky-Allen scheme, using only a few parameters (the charge trans- fer energy and the d d Coulomb interaction energy) is able to account for the electronic behaviour of a great number of 3d TM oxides such as the phase transitions. In order to find the empirical values for these energies for PNO, 2p-core X-ray absorption spectra were calculated within multiplet ligand field theory for the PNO single cluster. Then by adjusting the calculated spectra with the experiment, the best agreement happened at $\Delta = 2.5$ eV and pds=-1.9 eV. Changing the charge transfer energy and the covalent hopping integral mostly changes the L_3 double peak intensity ratio until it reaches the spin transition and changes the line shape drastically. Therefore, they mostly are chosen to satisfy this ratio to the most. Even though the best match was not satisfactory and differed with experiment in this ratio and the presence of a shoulder there. The differences are even more considerable for a smaller life-time broadening of 0.2 eV with multiple peaks present.

Then, the low spin to high spin state transition was studied and the critical values of Δ and pds at which the system experiences an abrupt spin transition were obtained. A map also was presented in which for any values of the charge transfer energy and covalent hopping integral the spin state can be predicted.

Then, another approach was employed to adjust these crucial parameters. The RIXS spectra were calculated in the same theory, basis set and ground state. In experimental RIXS, the first excitation peaks appeared at less than 1 eV. They were double peaked and showed polarization dependence at some resonant energies on the left side of the L_3. By calculating several RIXS spectra and corresponding the relative eigen-energies to the $d-d$ excitation peaks and considering the above features of the first observed inelastic peaks in the experiment, it was concluded that these first peaks in fact correspond to the second $d-d$ excitation in about 1 eV and the first excitation should have been in a very low energy lower than the experiment energy resolution (less than 0.1 eV).

The values which satisfies these energies (the second relative eigen-energy at less than 0.1 eV and the third one at about 1 eV) were found to be $\Delta = 0.8$, $tpp = 0.8$, $pds = -1.4, 10Dq = 0.4$, $U_{dd} = 7.5$, $U_{pd} = 9$ eV

Therefore, to get the best agreement with RIXS in terms of the $d-d$ excitation energies, the charge transfer energy and covalent hopping integral change a lot. These new values do not give the best agreement with XAS any more and the double peak on L_3 will be lost. However, the fact that even the best XAS match was not satisfactory at all and the fact that no RIXS

polarization dependence was found on the right side of the L_3 unlike the left side, and the fact that the resonant inelastic x ray scattering spectra extended out to an energy region including the second peak of the L_3 XAS demonstrate a linear dispersion with incident energy after having passed through the first peak demonstrates that the second peak has a very different origin and must involve a continuum state in which the excited electron in a state decoupled from the core hole and so does not participate in the decay to the core hole state and the true values for Δ and pds should not be obtained by keeping this second peak in L_3 in MLFT calculations.

There are some other reasons which might have caused the differences between the calculations and the experiment. In our calculations it has been shown that for almost all the low spin cases, the d^8L^9 configuration has the largest contribution in the ground state. It can suggest that the true starting point for this problem might be the starting point in which we start with nickel d^8 configuration and a hole in the oxygens and then we can no longer use a single local cluster because all the other nickels are also contributing ligand holes.

Here also for simplicity, the cubic symmetry and zero distortion have been assumed which is not exactly the case in the real material and might have caused the disagreements.

Bibliography

[1] Resonant inelastic x-ray scattering. `http://en.wikipedia.org/wiki/Resonant_inelastic_X-ray_scattering`, October 2013.

[2] Spherical coordinate system. `http://en.wikipedia.org/wiki/Spherical_coordinate_system`, October 2013.

[3] Martin Buschke. Orbital reconstruction at the surface of lanthanum nickelate thin films. *B.Sc thesis*, 2012.

[4] C. F. Chang, Z. Hu, Hua Wu, T. Burnus, N. Hollmann, M. Benomar, T. Lorenz, A. Tanaka, H.J. Lin, and H.H. Hsieh. Spin blockade, orbital occupation, and charge ordering in $La_{1.5}Sr_{0.5}CoO_4$. *Physical Review Letters*, 102(116401), 2009.

[5] Jew-Tin Chen. Coordination chemistry. `http://www.ch.ntu.edu.tw/~jtchen/course/inorganic/coord%20chem.html`, October 2013.

[6] A. Fujimori and F. Minami. *Physical Review B*, 30(957), 1984.

[7] Frank de Groot and Akio Kotani. *Core Level Spectroscopy of Solids*. CRC press, 2008.

[8] M.W. Haverkort, M. Zwirzycki, and O.K. Andersen. Multiplet ligand-field theory using wannier orbitals. *Physical Review B*, 85(165113), 2012.

[9] W. Maurits Haverkort. Spin and orbital degrees of freedom in transition metal oxides and oxide thin films studied by soft x-ray absorption spectroscopy. *PhD thesis*, 2005.

[10] S. Hufner. *Solid state Commun*, 49(1177), 1985.

[11] S Macke, A Radi, J. E. Hamann-Borrero, R. Sutarto, F. He, G. Logvenov, and G. Christiani. X-ray absorption spectrum. *Canadian Light Source and Stuttgart Max Planck Institute*.

[12] Dick van der Marel. The electronic structure of embedded transition metal atoms. *PhD thesis*, 1985.

[13] Maria Luisa Medarde. Structural, magnetic and electronic properties of rnio3 perovskites(r=rare earth). *J. Phys.: Condens. Matter 9*, (16791707), 1997.

[14] C.E. Moore. Atomic energy levels. *NBS Circular*, (467), 1949.

[15] C.N.R Rao. Transition metal oxides. *Annu. rev. phys. chem.*, 40(291-326), 1989.

[16] G.A Sawatzky and J.W. Allen. *Physical Review letter*, 53(2339), 1984.

[17] George Sawatzky. Electronic structure of correlated electron systems. `http://www.phas.ubc.ca/~berciu/TEACHING/PHYS555/FILES/`, September 2013.

[18] Attila Szabu and Neil S. Ostlund. *Modern Quantum Chemistry*. 1996.

[19] J.B. Torrance, P. Locorre, A.I. Nazzal, E.J. Ansaldo, and Ch. Niedermayer. Systematic study of insulator-metal transitions in perovskites $RNiO_3$(R=Pr,Nd,Sm,Eu) due to closing of charge-transfer gap. *Physical Review B*, 45(14), 1991.

[20] J. Zaanen. *PhD thesis*, 1986.

[21] J. Zaanen, G. A. Sawatzky, and J.W. Allen. Band gaps and electronic structure of transition-metal compounds. *Physical Review letters*, 55(4), 1985.

[22] J Zaanen, C. Westra, and G. A. Sawatzky. Determination of the electronic structure of transition-metal compounds: 2p x-ray photoemission spectroscopy of the nickel dihalides. *Physical Review B*, 33(12), 1986.

[23] Pavlo Zubko, Stefano Gariglio, Marc Gabay, Philippe Ghosez, and Jean-Marc Triscone. Interface physics in complex oxides heterostructures. *Annu. Rev. Condens. Matter Phys.*, 65(141), 2011.

Appendix

Here the resonant inelastic scattering spectra at various incident energies and with the charge transfer energy of 2.5 and 0.5 eV are presented. The photon energies are about the X-ray absorption L_3 peak. The vertical axis is the intensity in an arbitrary unit and the horizontal axis is the energy loss in eV. The descriptions can be found in the chapter 4 of this thesis.
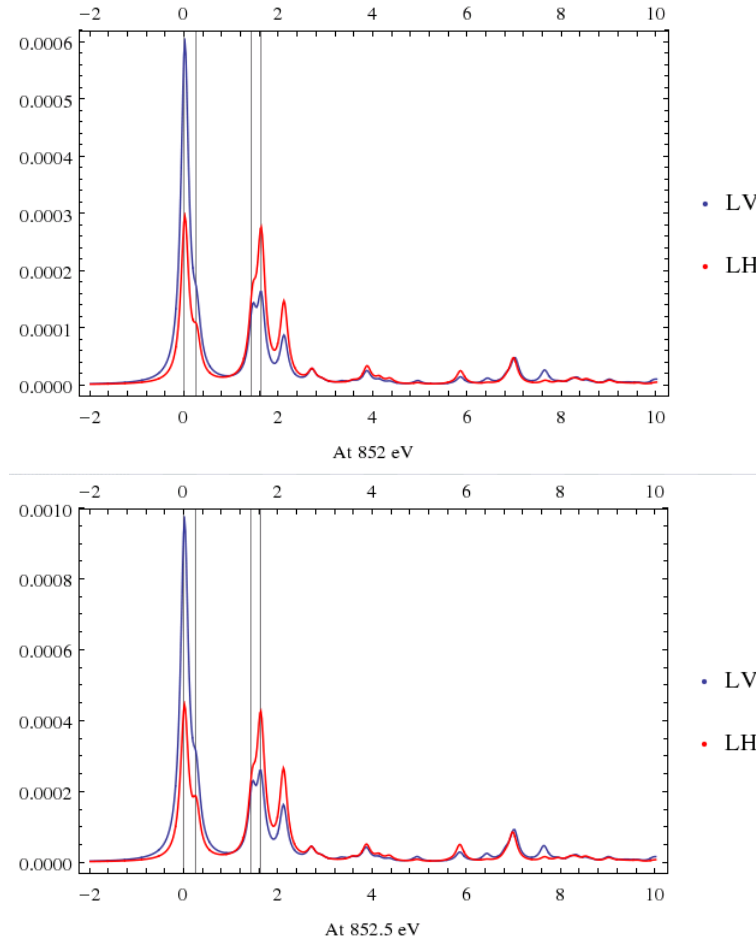

Figure 5.1: Calculated RIXS spectra with the following parameters: $\Delta = 2.5$, $tpp = 0.8$, $pds = -1.9, 10Dq = 0.5$, $U_{dd} = 7.5$, $U_{pd} = 9$ eV and RIXS broadening of 0.2 eV
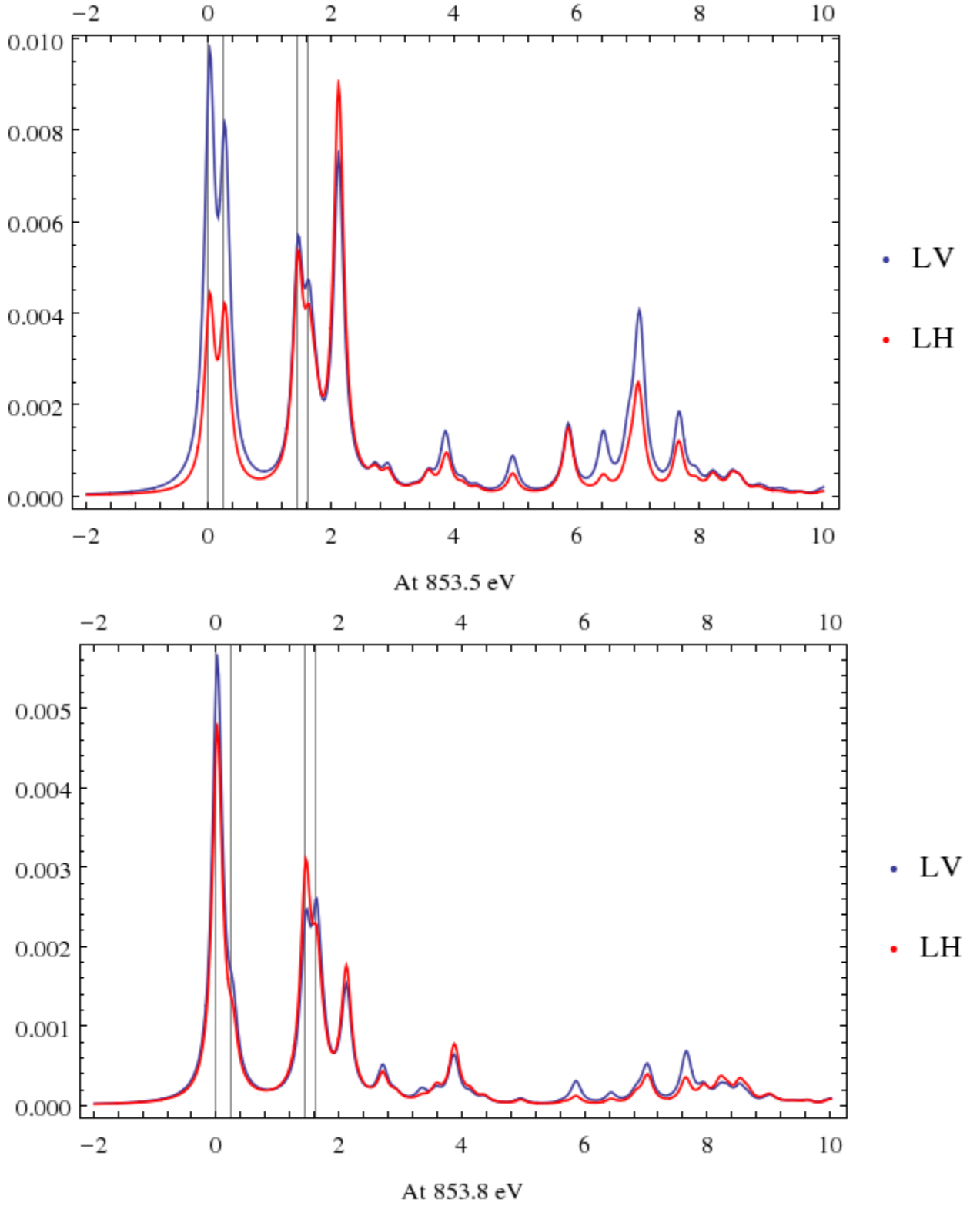
Figure 5.2: Calculated RIXS spectra with the following parameters: $\Delta = 2.5$, $tpp = 0.8$, $pds = -1.9$, $10Dq = 0.5$, $U_{dd} = 7.5$, $U_{pd} = 9$ eV and RIXS broadening of 0.2 eV
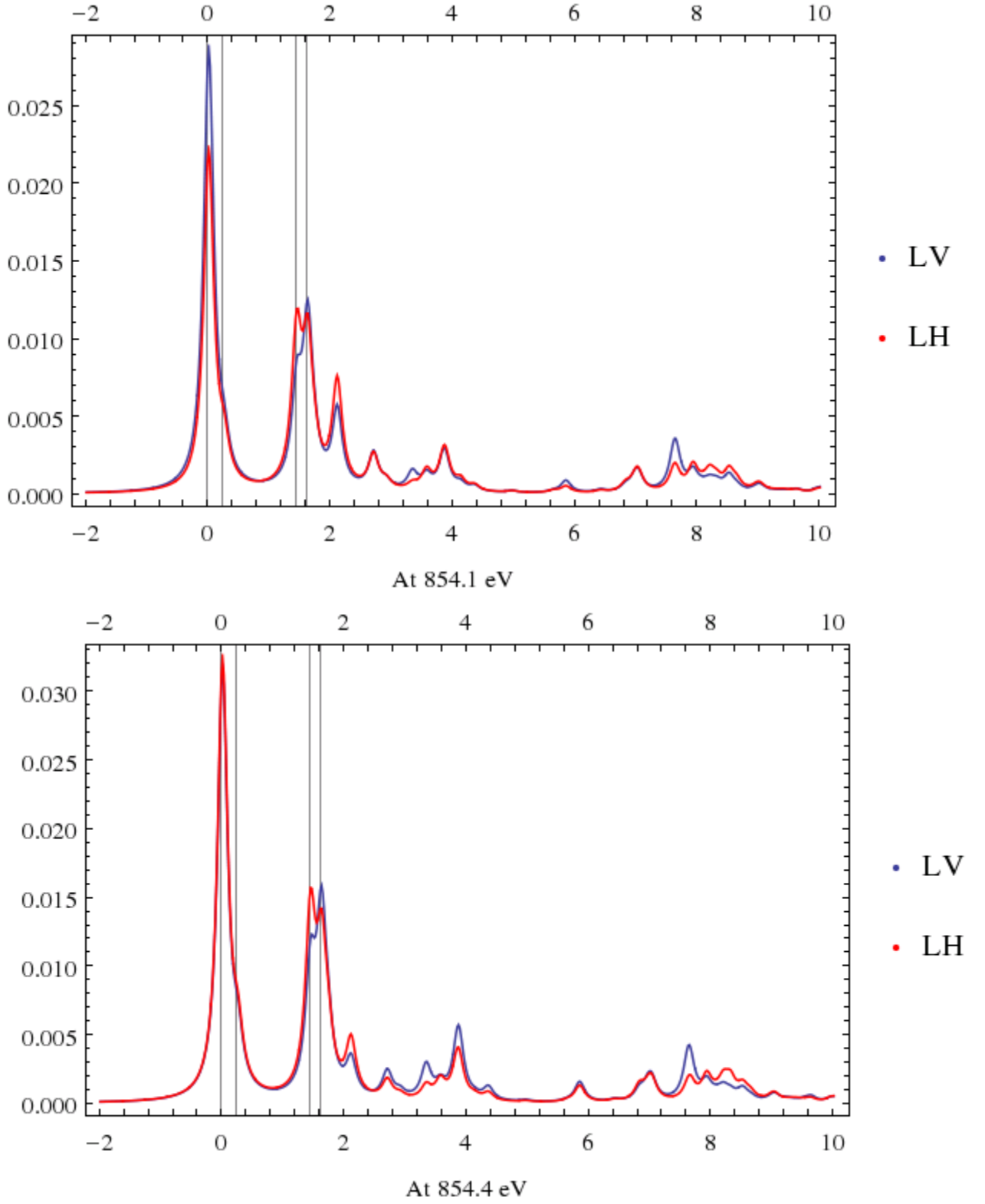
Figure 5.3: Calculated RIXS spectra with the following parameters: $\Delta = 2.5$, $tpp = 0.8$, $pds = -1.9$, $10Dq = 0.5$, $U_{dd} = 7.5$, $U_{pd} = 9$ eV and RIXS broadening of 0.2 eV
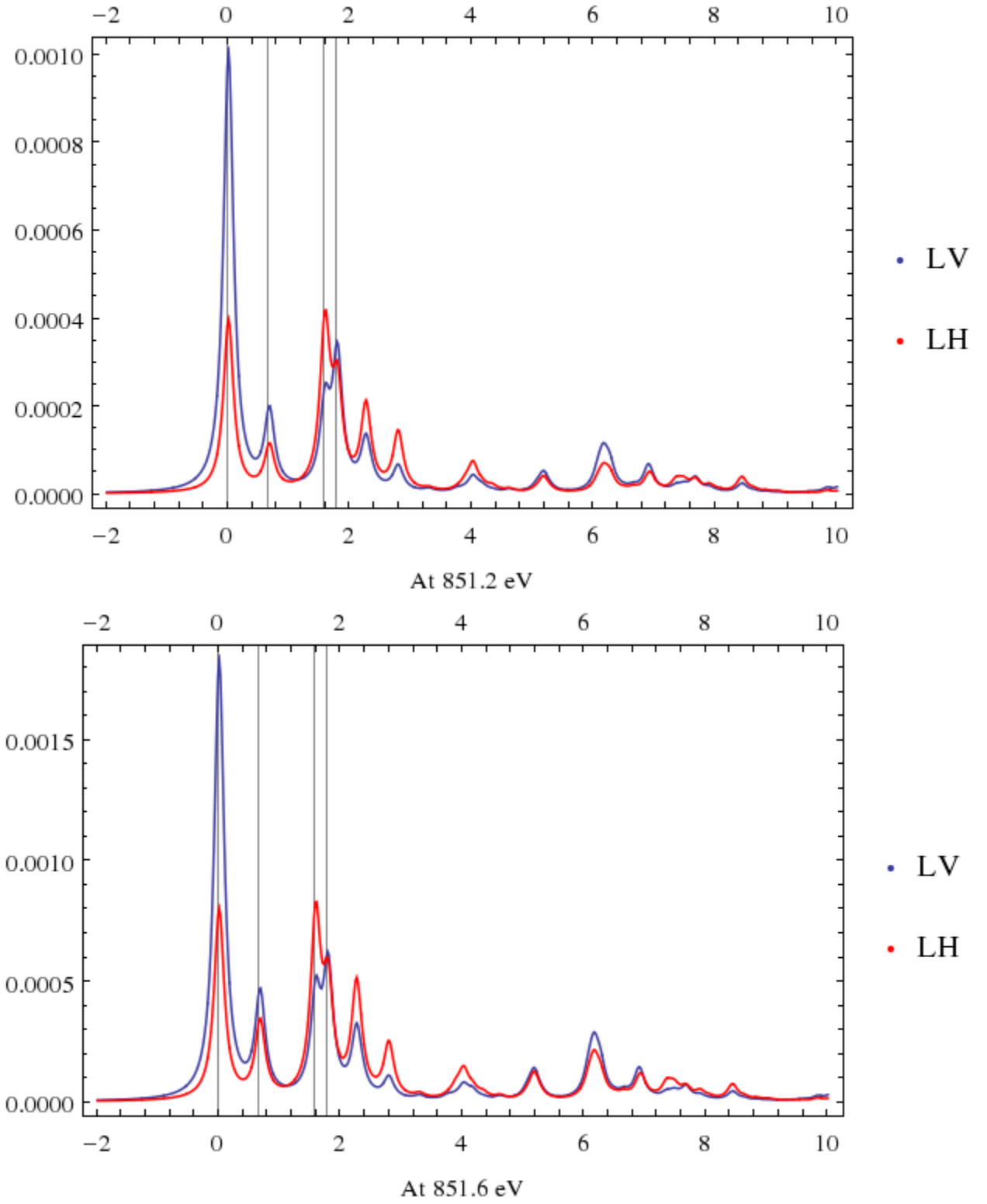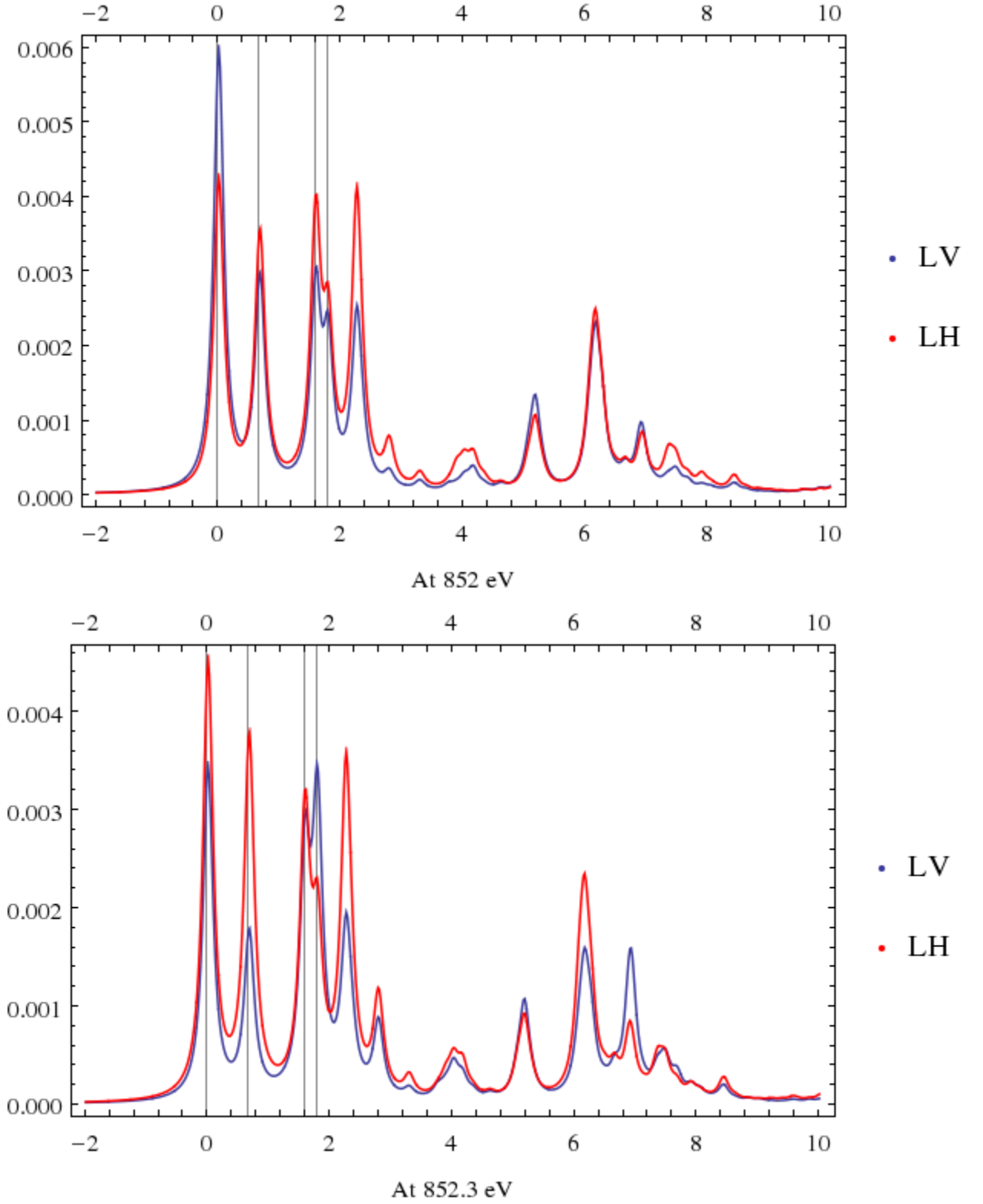
Figure 5.4: Calculated RIXS spectra with the following parameters: $\Delta = 0.5$, $tpp = 0.8$, $pds = -1.9$, $10Dq = 0.5$, $U_{dd} = 7.5$, $U_{pd} = 9$ eV

Figure 5.5: Calculated RIXS spectra with the following parameters: $\Delta = 0.5$, $tpp = 0.8$, $pds = -1.9$, $10Dq = 0.5$, $U_{dd} = 7.5$, $U_{pd} = 9$ eV
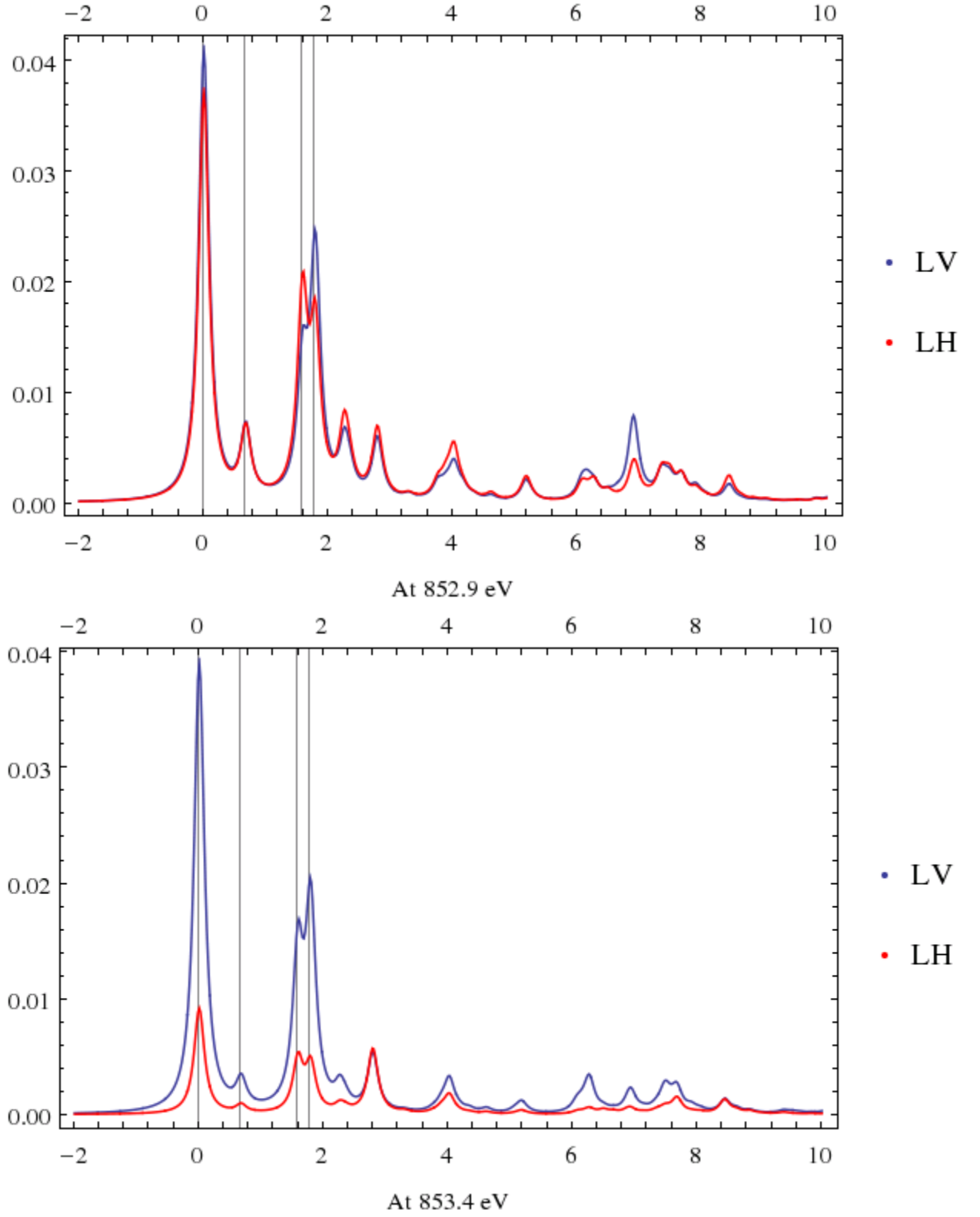
Figure 5.6: Calculated RIXS spectra with the following parameters: $\Delta = 0.5$, $tpp = 0.8$, $pds = -1.9$, $10Dq = 0.5$, $U_{dd} = 7.5$, $U_{pd} = 9$ eV
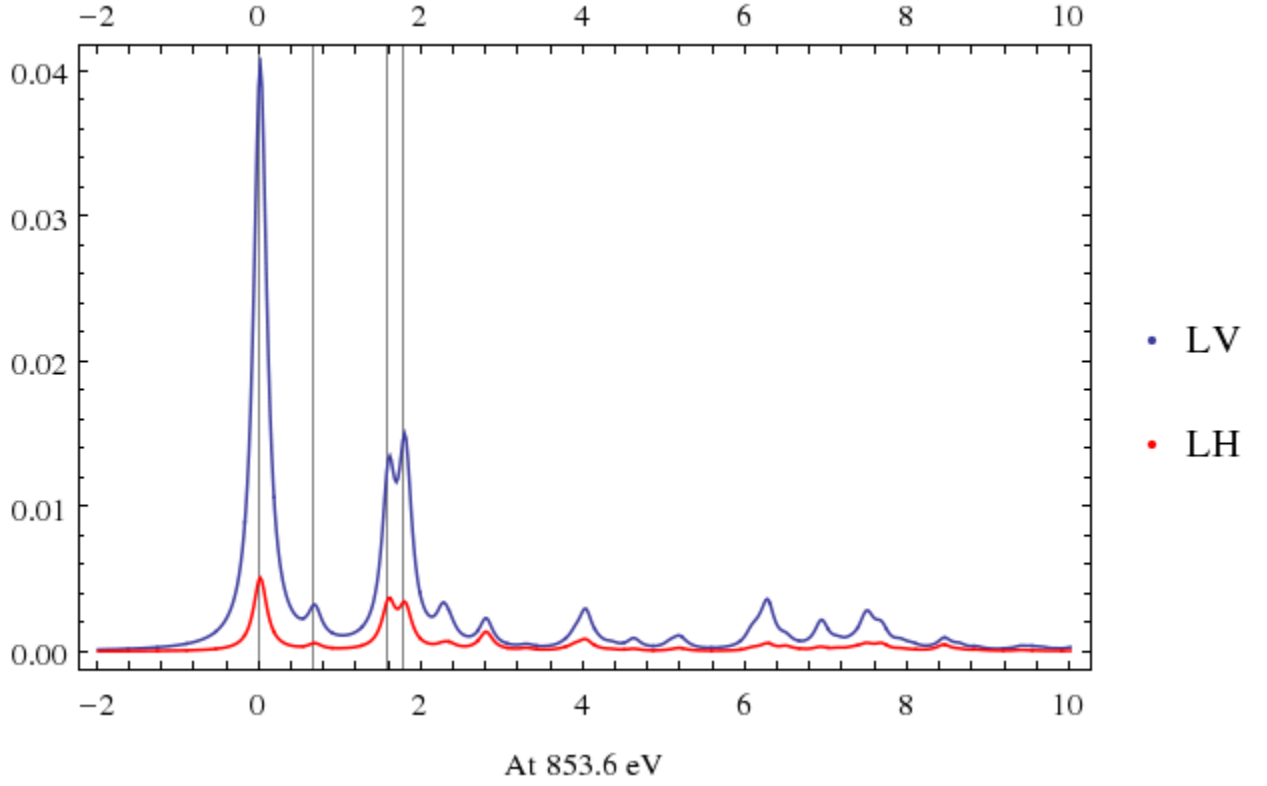
Figure 5.7: Calculated RIXS spectra with the following parameters: $\Delta = 0.5$, $tpp = 0.8$, $pds = -1.9, 10Dq = 0.5$, $U_{dd} = 7.5$, $U_{pd} = 9$ eV